Click Here for Full Article

Impacts of Argo salinity in NCEP Global Ocean Data Assimilation System: The tropical Indian Ocean

Boyin Huang,[1] Yan Xue,[2] and David W. Behringer[3]

[1]   Salinity profiles collected by the International Argo Project (International Argo Project data are available at http://argo.jcommops.org) since 2000 provide us an unprecedented opportunity to study impacts of salinity data on the quality of ocean analysis, which has been hampered by a lack of salinity observations historically. The operational Global Ocean Data Assimilation System (GODAS) developed at the National Centers for Environmental Prediction (NCEP) assimilates temperature and synthetic salinity profiles that were constructed from temperature and a local *T-S* climatology. In this study, we assess impacts of replacing synthetic salinity by Argo salinity on the quality of the GODAS ocean analysis with a focus on the tropical Indian Ocean. The study was based on two global ocean analyses for 2001–2006 with (NCEP_Argo) and without (NCEP_Std) inclusion of Argo salinity. The quality of the ocean analyses was estimated by comparing them with various independent observations such as the surface current data from drifters, the salinity data from the Triangle Trans-Ocean Buoy Network moorings, and the sea surface height (SSH) data from satellite altimeters. We found that by assimilating Argo salinity, the biases in the salinity analysis were reduced by 0.6 practical salinity units (psu) in the eastern tropical Indian Ocean and by 1 psu in the Bay of Bengal. Associated with these salinity changes, the zonal current increased by $30–40$ cm s^{-1} toward the east in the central equatorial Indian Ocean during the winter seasons. When verified against drifter currents, the biases of the annually averaged zonal current in the tropical Indian Ocean were reduced by $5–10$ cm s^{-1}, and the root-mean-square error of surface zonal current was reduced by $2–5$ cm s^{-1}. The SSH biases were reduced by 3 cm in the tropical Indian Ocean, the Bay of Bengal, and the Arabian Sea. These results suggest that the Argo salinity plays a critical role in improving salinity analysis, which in turn contributed to improved surface current and sea surface height analyses.

1.   Introduction

[2]   The National Centers for Environmental Prediction (NCEP) have been producing real-time ocean analysis and historical reanalysis using Ocean Data Assimilation System (ODAS) since 1995 [*Ji et al.*, 1995]. The ODAS was used to initialize the oceanic component of the NCEP's coupled ocean-atmosphere general circulation model and has been shown to improve the El Niño–Southern Oscillation (ENSO) forecast skill significantly [*Ji et al.*, 1995]. However, serious problems existed in ODAS, largely associated with a lack of salinity observations. *Acero-Schertzer et al.* [1997] showed that the model salinity distribution in ODAS

became nearly homogeneous, and the model currents differed significantly from the drifter current observations. The main reason for those errors is that neither freshwater flux forcings nor observed temperature-salinity correlations were maintained when temperature profile data were assimilated. A new operational Global Ocean Data Assimilation System (GODAS) was developed in 2004 [*Behringer and Xue*, 2004] and used to initialize the oceanic component of the NCEP's new Climate Forecast System [*Saha et al.*, 2006]. To reduce the salinity biases in the previous ODAS, the new GODAS assimilated synthetic salinity profiles that were constructed from temperature and a local *T-S* climatology because of the lack of salinity observations. The synthetic salinity has an advantage in improving the climatological salinity analysis but a disadvantage in seriously underestimating salinity variability in the intraseasonal and interannual timescales. The impacts of salinity variability on tropical Pacific oceanic circulations have been addressed using ocean general circulation models forced with salt fluxes [*Murtugudde and Busalacchi*, 1998; *Vialard et al.*,

---

[1]Wyle Information System/CPC, NCEP, NOAA, Camp Springs, Maryland, USA.
[2]CPC, NCEP, NOAA, Camp Springs, Maryland, USA.
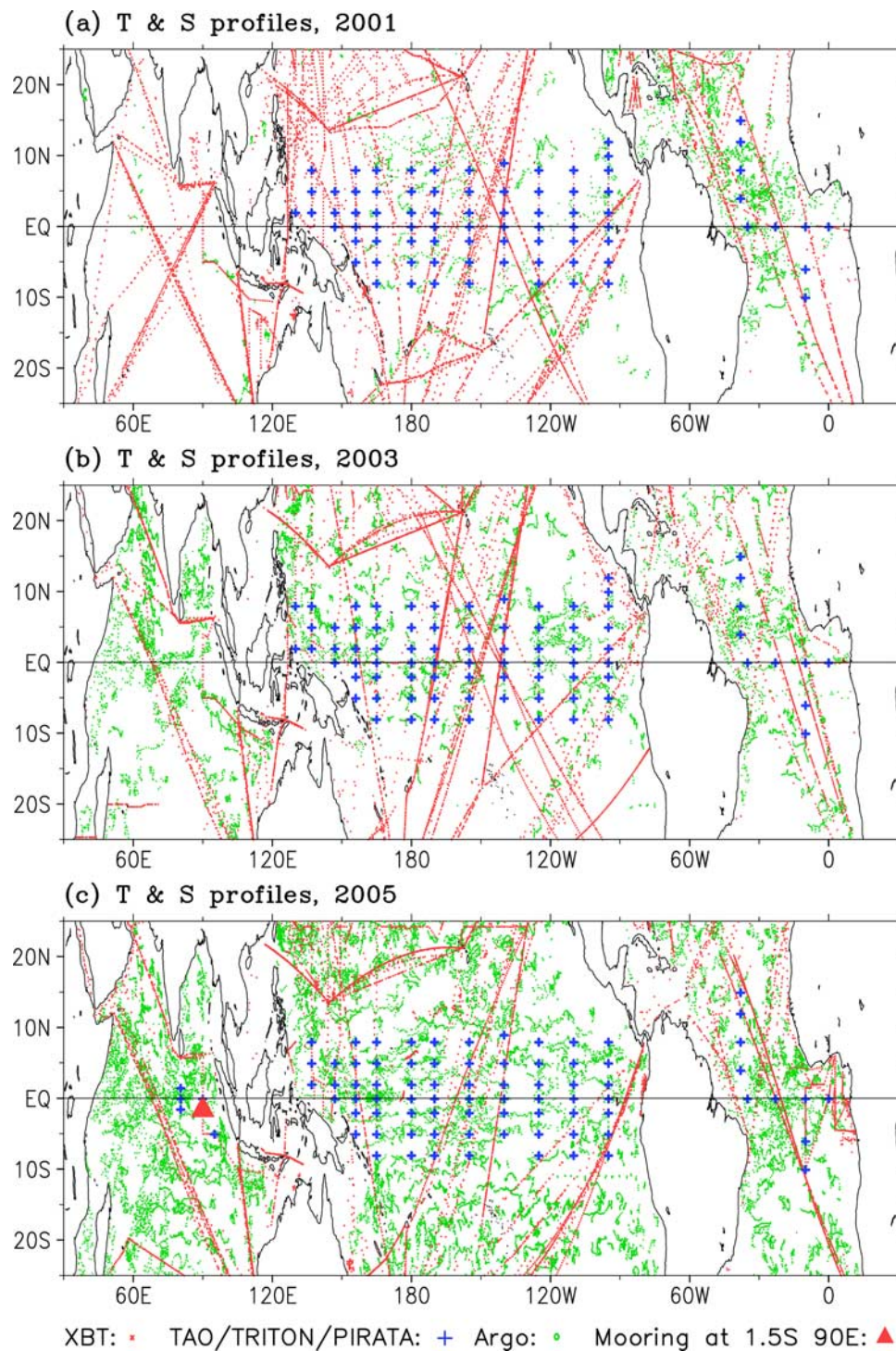[3]EMC, NCEP, NOAA, Camp Springs, Maryland, USA.

Figure 1. Distribution of temperature and salinity profiles used in National Centers for Environmental Prediction (NCEP) Global Ocean Data Assimilation System (GODAS) in (a) 2001, (b) 2003, and (c) 2005. One mark represents a monthly averaged vertical profile.

2002]. We suspect that the underestimation of salinity variability due to assimilation of the synthetic salinity has contributed to the large zonal current biases in the equatorial Pacific (see the validation skill at the GODAS website at http://www.cpc.ncep.noaa.gov/products/GODAS).

[3] The importance of including salinity observations in ocean data assimilation has been addressed by *Cooper* [1988] and *Woodgate* [1997]. However, salinity observa-

tions have been very sparse until recently, when the Argo data became available in 2000 [*Boutin and Martin*, 2006; *Gould and Turton*, 2006; *Gould et al.*, 2004]. Argo collects salinity and temperature profiles from near surface to 2000 m depth from a sparse (average $3° \times 3°$ spacing) array of robotic floats that populate the ice-free oceans. The spatial distribution of the Argo data varies with time, beginning with a good coverage for the Atlantic Ocean only in 2001,

gradually increasing its coverage for other ocean basins, and reaching a near-global coverage in 2006 (Figure 1).The Argo salinity observations provide us an unprecedented opportunity to improve the salinity analysis in GODAS.

[4] Two experimental GODAS runs have been made to assess impacts of the Argo salinity on the quality of the GODAS ocean analysis. Inclusion of Argo salinity data in GODAS has led to significant improvements in both salinity analysis and oceanic circulations. *Behringer* [2007] provided a description of these two experiments and other experiments that were designed as developmental runs for the next operational GODAS by including new observational data, such as the Argo salinity and altimetry sea level data and some renovations of the data assimilation scheme. He found that inclusion of the Argo salinity has led to dramatic improvements in the tropical Pacific zonal current analysis in 2005. Further study is needed to understand why the zonal currents were improved significantly and whether the improvements existed for other years.

[5] Compared to the tropical Pacific Ocean, the quality of the GODAS ocean analysis in the tropical Indian Ocean has been much less analyzed because of a lack of validation data. However, an accurate ocean analysis for the tropical Indian Ocean is desired not only for initialization of oceanic components of coupled general circulation models, but also for diagnostic study of climate-related oceanic processes in the region. On seasonal-to-interannual timescales, the so-called Indian Ocean dipole (IOD) [*Saji et al.*, 1999] events have drawn lots of research attention since they involve both thermodynamics and dynamic oceanic processes similar to those for ENSO, and it has significant impacts on the Indo-Pacific climate [*Saji and Yamagata*, 2003]. The tropical Indian Ocean is intimately connected to the tropical Pacific Ocean through the oceanic and atmospheric bridges, and its influences on ENSO and the Asia/Australia monsoon are yet to be fully understood [*Ashok et al.*, 2001; *Shinoda et al.*, 2004; *Behera and Yamagata*, 2003]. Therefore, it is important to have a good estimation of the quality of the GODAS ocean analysis in the tropical Indian Ocean for its climate applications.

[6] In this paper, we will analyze whether and how much the Argo salinity contributes to improvements of the GODAS ocean analysis in the tropical Indian Ocean. The paper is organized as follows: the operational GODAS and two experimental GODAS runs are described in sections 2 and 3, the validation data are described in section 4, the analysis of impacts of the Argo salinity is presented in section 5, and the summary is presented in section 6.

2. Operational GODAS

[7] The operational GODAS was developed on the basis of the earlier version of the ODAS configured for the Pacific Ocean [*Ji et al.*, 1995; *Behringer et al.*, 1998]. The GODAS uses the Geophysical Fluid Dynamics Laboratory modular ocean model version 3 [*Pacanowski and Griffies*, 1998] configured globally from 75°S to 65°N. Longitudinal resolution is 1°. Latitudinal resolution is 1/3° near the equator and gradually increases to 1° beyond 10°S and 10°N. The vertical level thickness is 10 m above 200 m depth and increases downward with a total of 40 levels. The model uses an explicit free surface, the Gent-McWilliams

isopycnal mixing [*Gent and McWilliams*, 1990], and the K-profile parameterization vertical mixing [*Large et al.*, 1994]. The model is forced by the momentum, heat, and freshwater (evaporation minus precipitation) fluxes from the NCEP atmospheric reanalysis 2 [*Kanamitsu et al.*, 2002]. These surface fluxes were further corrected by restoring the model temperature of the first layer (5 m) toward the optimal interpolation sea surface temperature (SST) analysis version 2 [*Reynolds et al.*, 2002] and restoring the model surface salinity toward the annual sea surface salinity climatology [*Conkright et al.*, 1999]. The restoring timescale is 5 and 10 days for temperature and salinity, respectively.

[8] The operational GODAS was implemented in 2004 [*Behringer and Xue*, 2004] and was used to initialize the oceanic component of the NCEP's Climate Forecast System [*Saha et al.*, 2006]. The GODAS provides an ocean analysis from 1979 to present with pentad and monthly outputs on a 1° × 1° grid. To provide the public an easy access to the GODAS data set and oceanic monitoring products derived from GODAS, a comprehensive GODAS website has been constructed and maintained by the NOAA's Climate Prediction Center (NOAA data are available at http://www.cpc.ncep.noaa.gov/products/GODAS).

[9] Observed temperature profiles that were assimilated into the operational GODAS are from the expendable bathythermographs (XBTs), the Tropical Atmosphere-Ocean (TAO) in the tropical Pacific, Triangle Trans-Ocean Buoy Network (TRITON) in the tropical Indian Ocean, the Pilot Research Moored Array in the Tropical Atlantic (PIRATA) [*McPhaden et al.*, 2001], and Argo profiling floats [*Argo Science Team*, 2001]. The XBT observations collected prior to 1990 were acquired from the National Oceanographic Data Center (NODC) [*Conkright et al.*, 1999], while the XBTs collected after 1990 were acquired from work by the *Operational Oceanography Group* [2006]. Because of the lack of salinity observations, synthetic salinity profiles that were constructed from temperature and a local *T-S* climatology were assimilated into GODAS.

[10] The GODAS uses a 3-D variational (3DVAR) assimilation scheme that was originally developed by *Derber and Rosati* [1989]. It was adopted for operational use at NCEP, where it has undergone further development to assimilate salinity profiles and satellite altimetry [*Behringer et al.*, 1998; *Ji et al.*, 2000; *Behringer and Xue*, 2004; *Behringer*, 2007]. For the case that is relevant to this study, where only temperature and salinity are assimilated, the 3DVAR scheme minimizes a functional,

$$\mathbf{I} = \frac{1}{2}\big(\mathbf{T}^T\mathbf{E}^{-1}\mathbf{T}\big) + \frac{1}{2}\Big\{[D(\mathbf{T}) - \mathbf{T}_0]^T\mathbf{F}^{-1}[D(\mathbf{T}) - \mathbf{T}_0]\Big\},$$

where the vector **T** represents the correction to the first-guess prognostic tracers (temperature and salinity) computed by the model, **E** is the first-guess error covariance matrix, $D(\mathbf{T}) - \mathbf{T}_0$ represents the difference between the tracer observations and the first guess, D is an interpolation operator that transforms the first-guess tracers from the model grid to the observation locations, and F is the observation error covariance matrix for the tracers. In the present system, the first-guess error covariance matrix, **E**, is univariate and thus block diagonal with respect to

Table 1. Data Sets Assimilated in NCEP_Std and NCEP_Argo[a]

Experiments	Temperature Data	Salinity Data
NCEP_Std	XBT	XBT, synthetic
	Argo	Argo, synthetic
NCEP_Argo	XBT	XBT, synthetic
	Argo	Argo, observed

[a]"Synthetic" means the salinity was calculated according to climatological temperature-salinity relationship and associated temperature profiles.

temperature and salinity. The horizontal covariance is modeled as a Gaussian function that is stretched in the zonal direction with the stretching being greatest near the equator. The vertical covariance is also modeled as a Gaussian function with a scale that increases with depth as the model grid separation increases; near the surface, the scale is approximately 25 m. The estimated first-guess error variance is scaled by the square root of the local vertical temperature gradient computed from a previous model analysis. In the present study, the current 5 day analysis provides the data for estimating the first-guess error variance for the next 5 day analysis. The observational errors are assumed to be uncorrelated, so that F is a diagonal matrix of the estimated error variances of the observations. The standard errors assigned to a temperature profile vary with depth according to the square root of the vertical temperature gradient and are scaled to have values between $1°C$ and $2.5°C$. In the operational GODAS, which assimilates synthetic salinity, a constant error estimate of 0.1 psu is assigned to the synthetic salinity profiles at all depths. These assigned error estimates are intended to account for the mismatch between the observations and the ocean model due to the effects of small-scale processes that are included in the observations but that are not resolved by the model. Further details of the assimilation method can be found in work by *Behringer et al.* [1998].

[11] Temperature and salinity profiles are assimilated at 12 h intervals, and the resulting corrections to the model temperature and salinity fields are added incrementally at each hourly model time step over the next 12 h. All profiles within a 2 week interval on either side of the time of the current assimilation cycle are included, but the more distant a profile is in time, the less weight it receives in the assimilation. This approach allows the relatively sparse ocean observations to have a greater impact on the model state [*Derber and Rosati*, 1989; *Behringer et al.*, 1998].

3. Experimental GODAS

[12] The standard GODAS (hereinafter referred to as NCEP_Std) (Table 1) is configured like the operational GODAS, except only temperature profiles from XBT, Argo, and associated synthetic salinity profiles were assimilated. To assess the impacts of the Argo salinity observations on the ocean analysis, the synthetic salinity profiles associated with Argo temperature profiles in NCEP_Std were replaced by Argo salinity profiles whenever they were available (NCEP_Argo). The temperature profiles from TAO/TRITON/ PIRATA and their associated synthetic salinity profiles, however, had not been assimilated in either NCEP_Std or NCEP_Argo. This is to prevent the impacts of Argo salinity from being overwhelmed by those of synthetic salinity since there are many more synthetic salinity profiles associated with temperature profiles from TAO/TRITON/PIRATA than Argo salinity profiles in the tropical oceans.

[13] We assigned 0.01 psu^2 as the error variance for observed Argo salinity profiles. Before we combined the synthetic and observed salinity profiles in the NCEP_Argo experiment, we increased the errors assigned to the synthetic salinity profiles. The purpose of increasing the errors assigned to the synthetic profiles is to reduce their weight relative to the observed profiles in the assimilation. To do this, we first binned the observed minus synthetic profile differences into 5° latitude by 10° longitude boxes and computed the mean and root-mean-square differences. These results were then mapped onto the model grid. Figure 2 shows these fields averaged at the surface and on the equator between 2000 and 2006, indicating that most of the differences occur in the upper 100 m above the halocline. The mapped fields were interpolated to the position of each synthetic profile, where the mean difference was added to the profile, and the square of the RMS difference was added to the error variance of 0.01 psu^2. The error variance assigned to the observed Argo salinity remained at the global value of 0.01 psu^2. Note that the assigned error variance to the synthetic profiles was as large as 0.17 psu^2 in the eastern tropical Indian Ocean and Bay of Bengal, which was more than 10 times of the error variance assigned to the Argo salinity profiles. In summary, whenever an Argo salinity profile coexisted with a synthetic salinity profile, the latter was mostly ignored by the model.

[14] The NCEP_Std and NCEP_Argo were run from 2001 to 2006, using the initial conditions from the operational GODAS in 2000. We will analyze the impacts of the Argo salinity on the ocean analysis by comparing NCEP_Std and NCEP_Argo between 2001 and 2006. Pentad (5 day) average outputs from those two ocean analyses were analyzed. The pentad averages are useful for direct comparison with observations that are mostly daily fields and can be used to study the impacts of Argo salinity on the intraseasonal variability.

4. Validation Data

[15] Independent observational data sets were collected to validate the ocean analyses in NCEP_Std and NCEP_Argo. The mooring salinity and temperature profiles at 1.5°S, 90°E from surface to 500 m from October 2001 to 2006 were acquired from NODC GTSPP [*Operational Oceanography Group*, 2006] and the TRITON Project (TRITON data are available at http://www.jamstec.go.jp/jamstec/TRITON/ real_time/top.html). The TRITON mooring also reported horizontal currents at 10 m, which were used to validate the horizontal currents in the two ocean analyses. The original NODC GTSPP and TRITON profiles were daily averaged data. They were processed into pentad averages and compared with the outputs from NCEP_Std and NCEP_Argo.

[16] Observed currents were collected and used to validate whether the changes in horizontal ocean currents between NCEP_Std and NCEP_Argo reflected a true improvement. The drifter current observations with drogues at
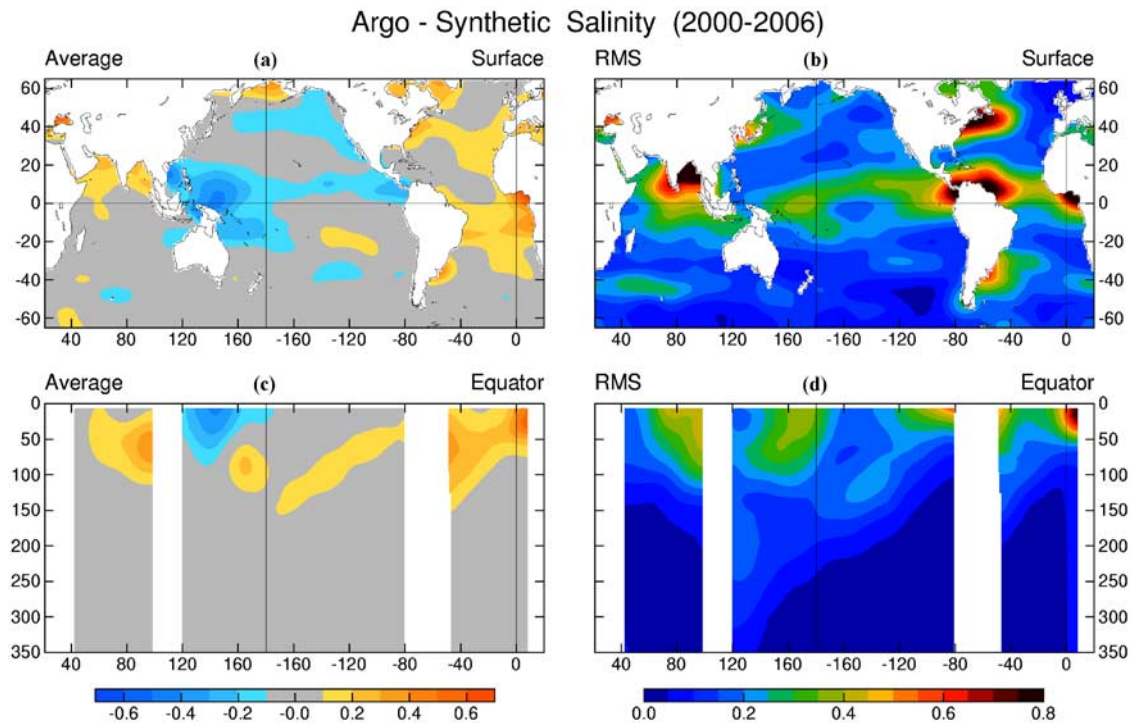
Figure 2. (a) Difference of Argo-observed and synthetic salinity at the surface between 2000 and 2006. Contour intervals are 0.1 practical salinity units (psu). (b) Same as Figure 2a except for RMS. Contour intervals are 0.05 psu. (c) Same as Figure 2a except for along the equator. (d) Same as Figure 2b except for along the equator.

15 m (hereinafter referred to as Drifter) from January 2001 to August 2006 were acquired from the Atlantic Oceanographic and Meteorological Laboratory (Atlantic Oceanographic and Meteorological Laboratory data are available at http://www.aoml.noaa.gov/phod/dac/gdp.html). The original 6 h-averaged drifter data were processed into daily averages if there were four valid observations within 24 h. The original observations designated as "drogue-off" were excluded. The daily averages were further processed into pentad averages if there were five valid daily averages within a pentad period.

[17] Ocean Surface Current Analysis-Real Time (OSCAR) [*Bonjean and Lagerloef*, 2002; *Johnson et al.*, 2007] currents were also used to validate the model currents. The OSCAR currents consisted of geostrophic velocity calculated from satellite altimetry sea level data, the Ekman velocity calculated from surface winds, and the velocity associated with the surface buoyancy gradient. The OSCAR currents are global from 70°S to 70°N with resolutions of 1° × 1° in latitude/longitude and 5 days in time from 1992 to present. The current data were linearly interpolated into daily data, and pentad-averaged currents were calculated using the daily data. Because of their full coverage in space and time, the OSCAR currents can be used to validate the model currents where and when the drifter currents were not available.

[18] The sea surface height (SSH) observations from satellite altimeters (hereinafter referred to as Altimetry) were used as independent observations since they were not assimilated into either NCEP_Std or NCEP_Argo. The daily SSH data, which have been derived in the form of

absolute dynamic topography from merged satellite altimeters of TOPEX, POSEIDON, Jason, and mean topography data, were acquired from Aviso segment sol multimission d'altimétrie, d'orbitographie et de localization precise and Developing Use of Altimetry for Climate Studies (Aviso segment sol multimission d'altimétrie, d'orbitographie et de localization precise and Developing Use of Altimetry for Climate Studies data are available at http://www.aviso.oceanobs.com). Pentad averages were calculated from daily data and were then compared with the pentad SSH of the ocean analyses between 2001 and 2006.

5. Impacts of Argo Salinity
5.1. Salinity and Temperature

[19] The differences in salinity between NCEP_Argo and NCEP_Std showed the direct impacts of assimilating the Argo salinity. Figure 3 shows the mean salinity differences at 50 m depth as well as the temperature profile distribution for each year in 2001–2006. It is seen that there were large increases in salinity at 50 m depth in the Bay of Bengal (0.4–0.8 psu), Arabian Sea (0.2 psu), and tropical eastern Indian Ocean (0.2–0.4 psu) after 2002 because of assimilating the Argo salinity (Figure 3). The large salinity changes between 2003 and 2006 are directly associated with a rapid increase of the areal coverage of the Argo salinity observations in the region (Figure 4). The areal coverage is calculated as follows: the tropical Indian Ocean (25°S–25°N, 40°E–105°E) is divided into 1° longitude and 1° latitude boxes. A box is marked as observed if one or more Argo profiles were found within the box in a particular
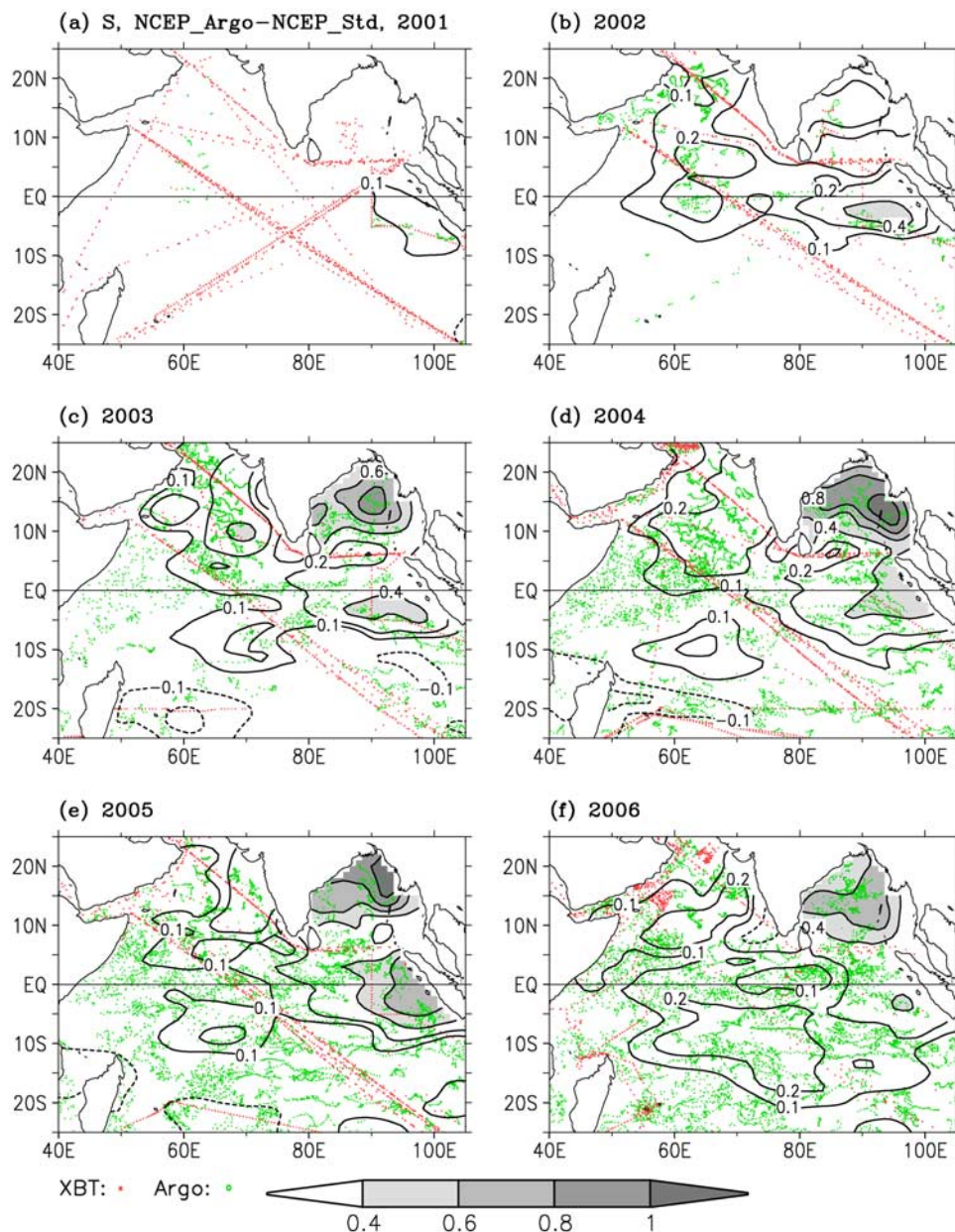
Figure 3. Annually averaged salinity difference at 50 m between NCEP_Argo and NCEP_Std in (a) 2001, (b) 2002, (c) 2003, (d) 2004, (e) 2005, and (f) 2006. The contours are ±0.1, ±0.2, ±0.4, ±0.6, ±0.8, and ±1 psu, respectively. Contours higher than 0.4 psu are shaded. Negative contours are dashed. Monthly profiles of expendable bathythermographs (XBT) and Argo temperature observations are overlapped.

month. The areal coverage of the month is defined as the ratio between the number of observed boxes and the number of all boxes in the region. Although the monthly areal coverage has increased monotonically since 2002, only about 14% of the tropical Indian Ocean has been observed in each month of 2006 (Figure 4).

[20] Further analysis indicated that the salinity changes were largely confined in the upper 100 m and were the largest near 50 m. As an example, Figure 5 shows the vertical sections of the salinity differences between NCEP_Argo and NCEP_Std along the equator (Figure 5a)

and 90°E (Figure 5b) in 2005. These salinity differences between NCEP_Argo and NCEP_Std are consistent with the differences between observed Argo salinity and synthetic salinity shown in Figures 2a and 2c.

[21] We need to verify, however, that the large salinity increases shown in Figures 3 and 5 truly represent an improvement in the salinity analysis. Figure 6a shows the salinity variability at the top 150 m measured at the TRITON mooring at 1.5°S, 90°E from October 2001 to December 2006. The differences between NCEP_Std and TRITON and between NCEP_Argo and TRITON are

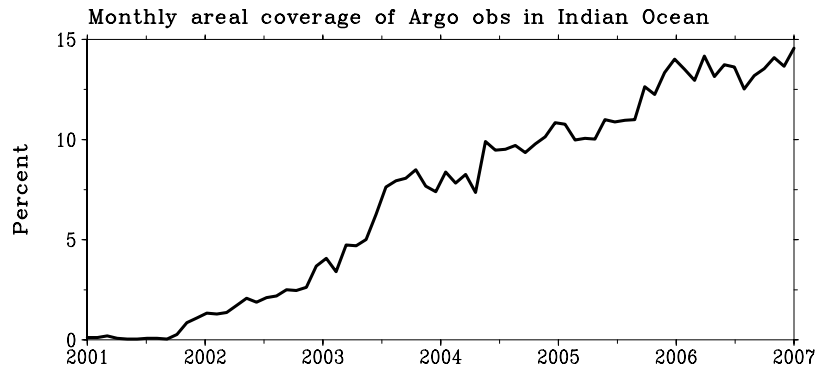**Monthly areal coverage of Argo obs in Indian Ocean**

Figure 4. Monthly areal coverage (in percent) of Argo observations in the Indian Ocean (25°S–25°N, 40°E–105°E). Annual areal coverage is 2, 12, 34, 45, 54, and 60% in 2001, 2002, 2003, 2004, 2005, and 2006, respectively.
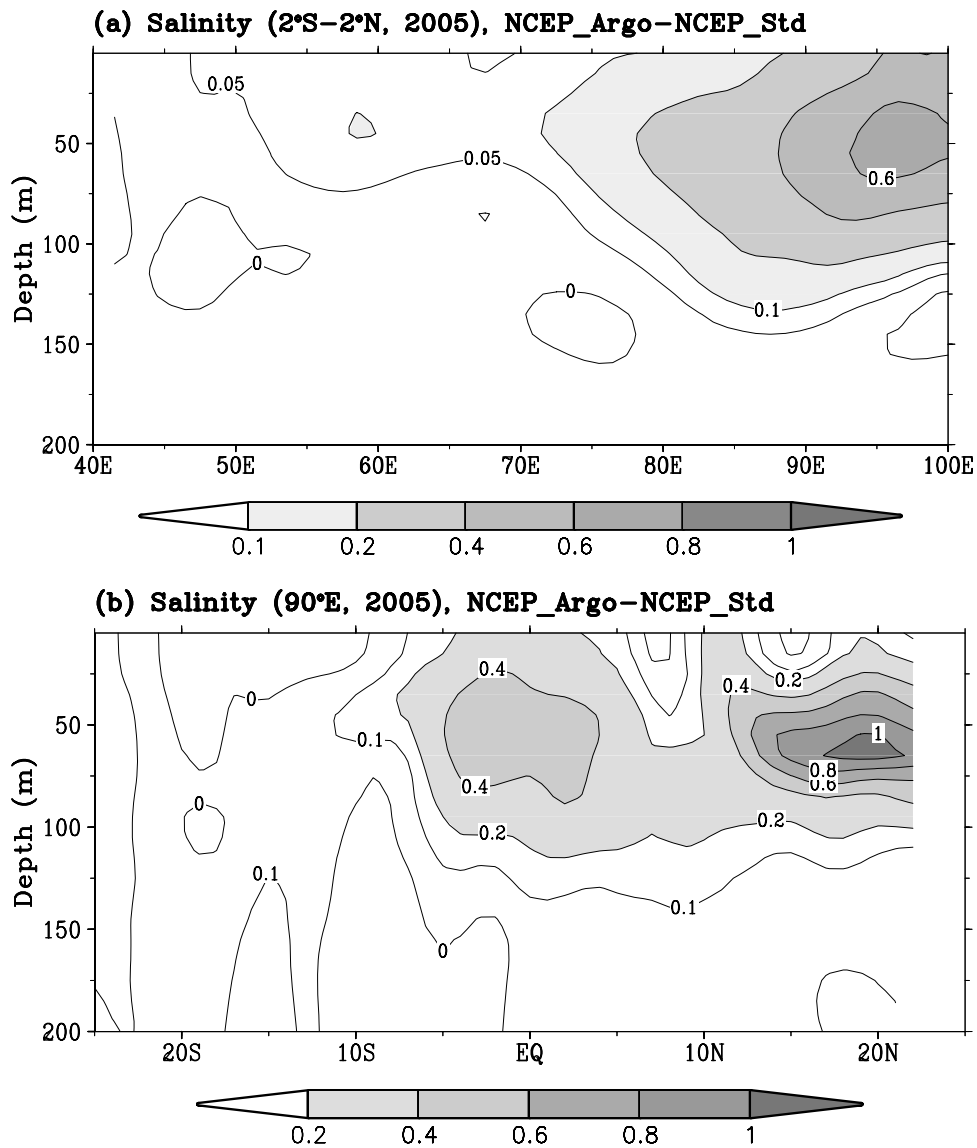
(a) Salinity (2°S–2°N, 2005), NCEP_Argo–NCEP_Std

(b) Salinity (90°E, 2005), NCEP_Argo–NCEP_Std

Figure 5. Annually averaged salinity difference between NCEP_Argo and NCEP_Std in 2005 along (a) equator and (b) 90°E. The contours are 0, 0.05, 0.1, 0.2, 0.4, and 0.6 psu in Figure 5a and 0, 0.1, 0.2, 0.4, 0.6, 0.8, and 1 psu in Figure 5b. Contours larger than 0.1 psu in Figure 5a and 0.2 psu in Figure 5b are shaded.
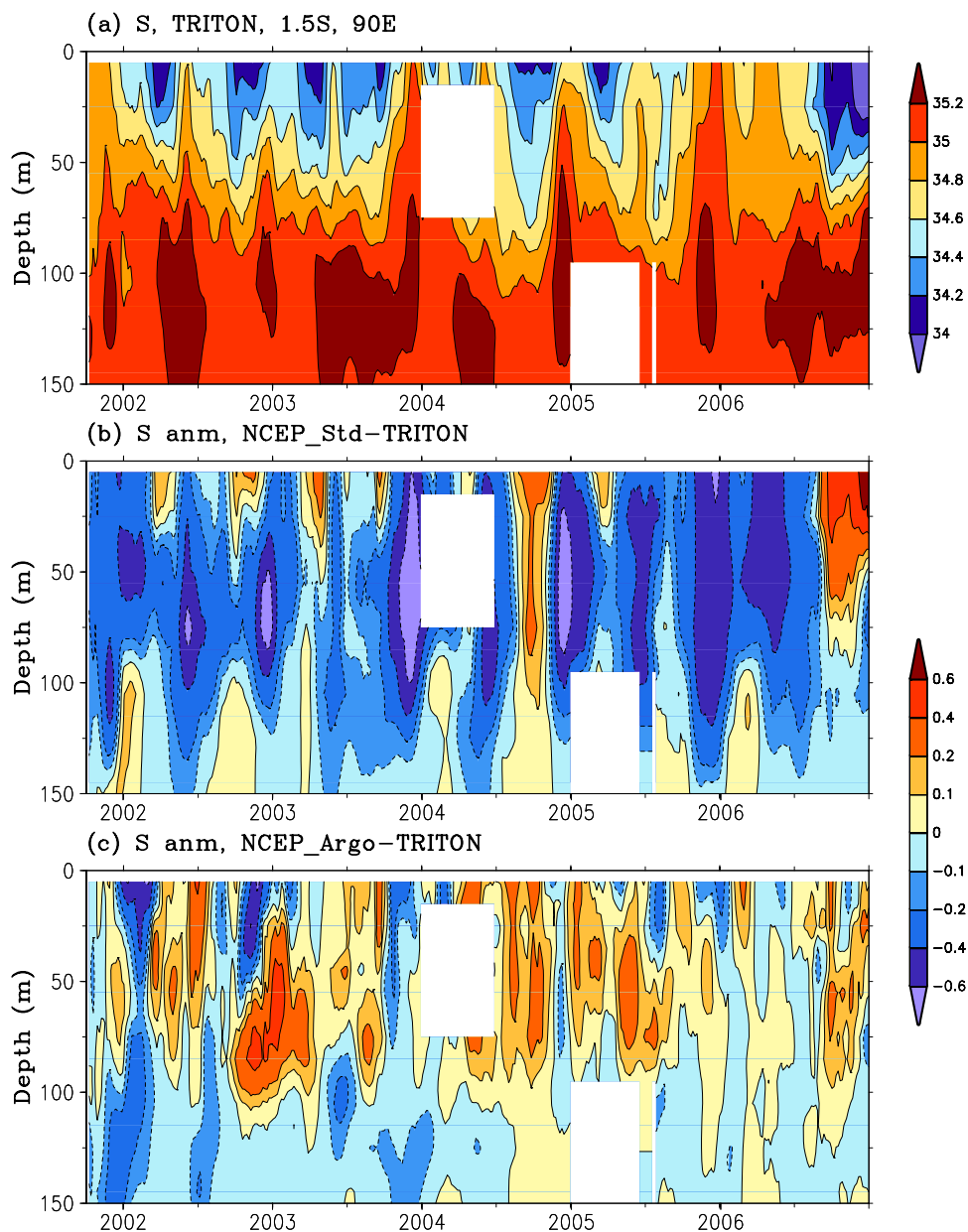
Figure 6. Five day (pentad) averaged salinity (psu) at 1.5°S, 90°E in (a) Triangle Trans-Ocean Buoy Network (TRITON), (b) NCEP_Std, and (c) NCEP_Argo. Contour intervals are 0.2 psu in Figure 6a, and contours are 0, ±0.1, ±0.2, ±0.4, and ±0.6 psu.

shown in Figures 6b and 6c. It is seen that the salinity in NCEP_Std was systematically lower (0.2–0.6 psu) than that in TRITON during the entire analysis period between 2002 and 2006, except for September 2004 and September–December 2006, when positive salinity biases were identified. Figure 6c indicated that the salinity in NCEP_Argo was much closer to the observations than NCEP_Std was during this period. The root-mean-square difference from the observations for the top 150 m is 0.3 psu in NCEP_Std and 0.18 psu in NCEP_Argo. The comparison suggests that the large salinity changes due to assimilation of the Argo salinity probably have resulted in a more accurate salinity analysis, although we do not have independent salinity observations to verify the salinity analysis over most of the Indian Ocean. The temperature changes due to assimilation

of the Argo salinity were generally small (not shown), which is not surprising since the same temperature profiles had been assimilated into NCEP_Std and NCEP_Argo.

[22] The large salinity correction above 150 m depth achieved by assimilating the Argo salinity also resulted in an improvement of the climatological barrier layer thickness (BLT) (Figure 7), which is measured as the difference between an isotherm depth and a mixed layer depth [*Sprintall and Tomczak*, 1992]. The mean BLT in NCEP_Argo was about 5–10 m thicker than that of NCEP_Std in the eastern tropical Indian Ocean and agreed with the mean BLT of *Conkright et al.* [2002] much better than that of NCEP_Std did (Figure 7). The increased BLT in NCEP_Argo was largely because of a reduction of the mixed layer depth
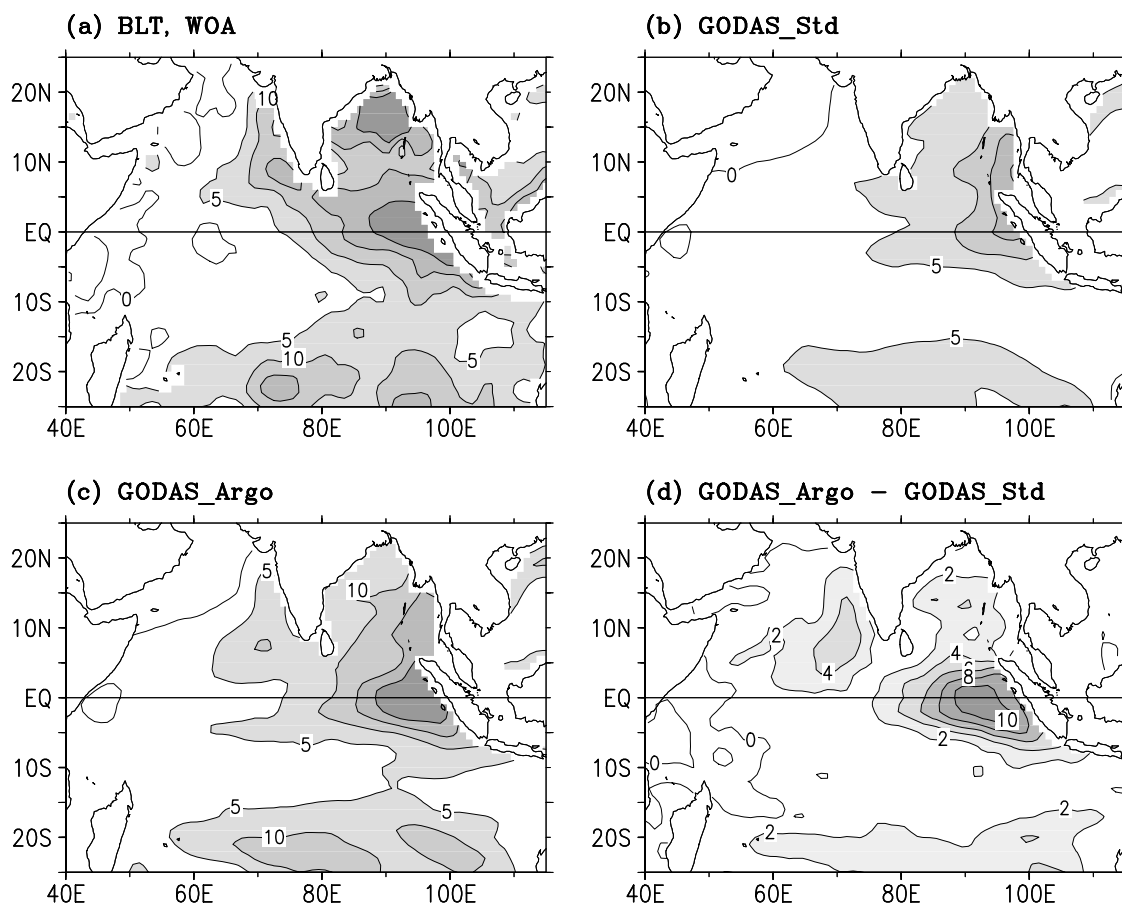
Figure 7. Barrier layer thickness in (a) *Conkright et al.*'s [2002] observations, (b) NCEP_Std, and (c) NCEP_Argo. (d) Barrier layer thickness difference between NCEP_Argo and NCEP_Std. Contour intervals are 5 m in Figures 7a, 7b, and 7c, and they are 2 m in Figure 7d.

resulting from an increase of salinity around 50 m depth (Figure 5).

5.2. Surface Currents

[23] The large salinity changes due to assimilation of the Argo salinity led to changes in the density gradient, which then would result in ocean current adjustment [*Huang and Mehta*, 2004, 2005; *Huang et al.*, 2005, and references therein]. It is indeed the case that assimilation of the Argo salinity induced significant changes in the surface currents in the equatorial Indian Ocean. Considering that the surface currents in the tropical Indian Ocean are largely zonal, we focused our analyses on the zonal currents. Figure 8 shows that the differences of the equatorial surface zonal currents between NCEP_Argo and NCEP_Std were mostly eastward during 2001−2006. The differences were as large as 30−40 cm s^{-1} during the winter season (December−February) of 2002, 2003, 2004, and 2005. In addition, a westward difference of 30−40 cm s^{-1} was found during June−August of 2002.

[24] To verify if the changes had led to improvements in the surface currents, the model currents were compared with the independent drifter currents from January 2001 to August 2006 (Figure 9). Figure 9 shows the drifter distributions for pentad observations within each individual year. The number of pentad observations is 161, 150, 158, 142,

210, and 171 in 2001, 2002, 2003, 2004, 2005, and 2006, respectively. The pentad-averaged currents were interpolated into regular 5° longitude and 1° latitude bin averages. To make the comparison fair, the pentad-averaged currents from NCEP_Std and NCEP_Argo were first interpolated into the grids of each pentad drifter in space and time and then were processed into 5° longitude and 1° latitude bin averages. This guarantees that the currents in the ocean analyses had the same sample rates as the drifters did and therefore reduced the sampling biases during the comparison of the gridded fields.

[25] Since the drifter observations are very sparse in time, we first compared the annually averaged currents. Figure 10a shows that the annually averaged currents were eastward at 10−30 cm s^{-1} in the equatorial Indian Ocean, which was in favor of the Wyrtki Jet [*Wyrtki*, 1973] in spring (April− June) and fall (October−December). The averaged currents were eastward at 10−20 cm s^{-1} near 5°S. The averaged currents were westward at 10−20 cm s^{-1} between 20°S and 10°S, which corresponded to the South Equatorial Current. The annually averaged zonal currents in NCEP_Std (Figure 10b) and NCEP_Argo (Figure 10c) were overall consistent with those of the drifter currents. The major differences were that in both NCEP_Std and NCEP_Argo, the zonal current in the equatorial Indian Ocean between 55°E and 75°E was westward, but it was eastward in Drifter; and the eastward current in the eastern equatorial Indian Ocean was
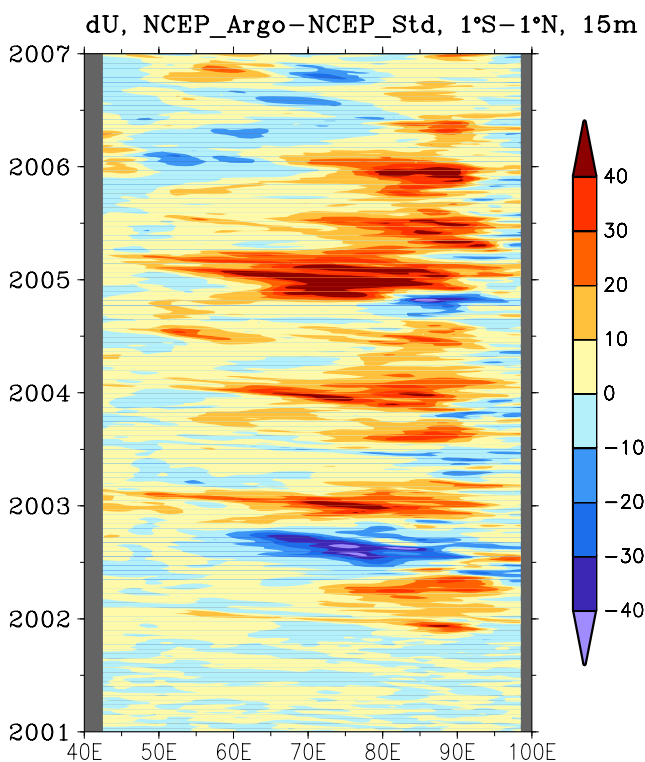
Figure 8. Zonal current difference in the equatorial (1°S–1°N) Indian Ocean at 15 m depth between NCEP_Argo and NCEP_Std. Units are cm s^{-1}.

weaker than that in Drifter; the eastward current near 5°S between 45°E and 80°E was stronger than that in Drifter. These biases are shown clearly by negative differences between NCEP_Std (or NCEP_Argo) and Drifter near the equator and positive differences near 5°N, 5°S, and south of 10°S (Figures 10d and 10e). These biases, however, had been reduced by 5–10 cm s^{-1} in NCEP_Argo (Figure 10f), which could be seen clearly by the opposite signs of the differences in Figures 10d and 10f. The improvement in zonal current, albeit small in the annual average, was found in the regions of the Wyrtki Jet. The improvement could also be seen from the reduction of RMS of anomalous zonal current (Figure 11c) between NCEP_Std and Drifter (Figure 11a) and between NCEP_Argo and Drifter (Figure 11b). The reductions in both annual average and RMS (2–5 cm s^{-1}) of anomalous zonal current suggest an improvement of zonal currents of about 5 cm s^{-1} in the tropical Indian Ocean.

[26] The comparison with the annually averaged (2001–2006) zonal current at 15 m from OSCAR indicates (not shown) that the spatial structure of the current is very similar to that of the drifter currents shown in Figure 10a. The differences between model simulations and OSCAR are very similar to those between model and drifter currents. Likewise, the changes in the averaged zonal currents and its RMS caused by assimilating the Argo salinity were about 5 cm s^{-1} in the tropical Indian Ocean, which effectively reduced the biases exhibited in NCEP_Std.

[27] The eastward zonal current changes between NCEP_Argo and NCEP_Std appear to be associated with the positive salinity changes in the eastern tropical Indian Ocean (Figure 3), which formed an eastward gradient of density along the equator. The higher salinity (and therefore higher density and lower SSH) generated a downwelling in the east and induced an eastward anomalous zonal current near the surface and westward anomalous zonal current in the subsurface (not shown). For example, the salinity difference between NCEP_Argo and NCEP_Std in the eastern Indian Ocean increased from 0.4 psu in 2004 (Figure 3d) to 0.6 psu in 2005 (Figures 3e and 5a). Associated with the salinity increase, the eastward zonal current changes between NCEP_Argo and NCEP_Std increased significantly from 2004 to 2005 (Figure 8). This is demonstrated clearly in the averaged (5°S–5°N and 70°E–80°E) zonal current during December 2004 and March 2005 (Figure 12a). The North Equatorial Current (NEC), which is westward in winter (January–March) and summer (July–September) but eastward in spring and fall (also referred to as Wyrtki Jet), was reduced and was closer to the observations in NCEP_Argo than in NCEP_Std. The reduction in NEC was largely associated with the increase of salinity gradient between the eastern (80°E–90°E, 5°S–5°N, 5–50 m) and western (50°E–60°E) tropical Indian Ocean (Figure 12b). We note that the westward zonal current differences during June–August of 2002 were also large (Figure 8). However, we were unable to validate it because of a lack of drifter observations during that season. The analysis in 2001–2002 may be less reliable than that in 2003–2006 because of a lack of Argo salinity.

[28] It is well known that the zonal currents in the tropical Indian Ocean exhibit a strong semiannual cycle [*Schott and McCreary*, 2001, and references therein]. The seasonal cycle of the zonal current in NCEP_Std, NCEP_Argo, and Drifter were assessed using 6 year data between 2001 and 2006. Our analysis (not shown) indicated that the NEC in the equatorial Indian Ocean during January–March and during July–August was too strong in NCEP_Std and was made closer to observations in NCEP_Argo. This can be seen in Figures 8 and 12. The changes in Wyrtki Jet between NCEP_Argo and NCEP_Std in the spring and fall seasons were not as large as those in the NEC in the winter and summer seasons.

[29] Since the drifter data were very sparse in space and time, they are not useful to assess the interannual variability of surface currents. The TRITON observations at (1.5°S, 90°E), however, provide continuously daily current measurements at 10 m depth between 2001 and 2006. The zonal currents from NCEP_Std, NCEP_Argo, and OSCAR were interpolated into the TRITON location at 1.5°S, 90°E and then compared with the TRITON currents. The comparison indicated that the seasonal and interannual variations of zonal currents at 1.5°S, 90°E were reasonably simulated by NCEP_Std and NCEP_Argo (Figure 13). The mean bias in NCEP_Argo is slightly larger than that in NCEP_Std, but the RMS and correlation with observations show a superiority of NCEP_Argo over NCEP_Std (Table 2). The mean bias and RMS in OSCAR are much larger than those in NCEP_Argo and NCEP_Std, but its correlation is superior to that of the two ocean analyses. The results suggest that the zonal current analysis of GODAS was improved by assimilating the Argo salinity, and its accuracy is comparable to that of OSCAR. However, the quality of the surface
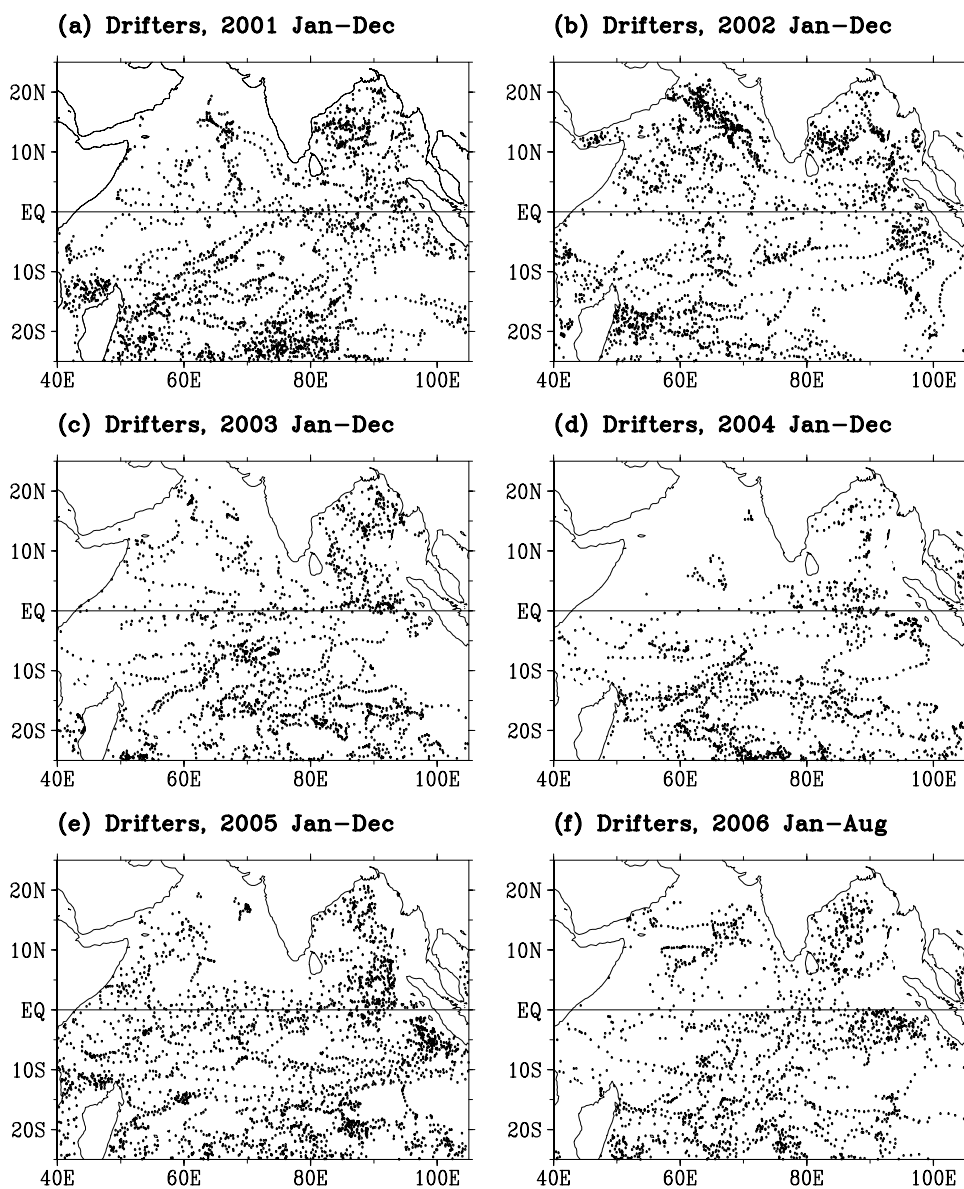
(a) Drifters, 2001 Jan–Dec   **(b) Drifters, 2002 Jan–Dec**

(c) Drifters, 2003 Jan–Dec   **(d) Drifters, 2004 Jan–Dec**

(e) Drifters, 2005 Jan–Dec   **(f) Drifters, 2006 Jan–Aug**

Figure 9. Distribution of drifter observations at 15 m depth in (a) 2001, (b) 2002, (c) 2003, (d) 2004, (e) 2005, and (f) 2006. One dot in the figure represents 5 day (a pentad) observations. The observations in 2006 were available from January to August.

current analysis cannot be verified over most of the tropical Indian Ocean because of a lack of validation data.

5.3. Sea Surface Height

[30] The large salinity changes from assimilation of the Argo salinity are expected to have direct impacts on SSH through their influences on density. Since the SSH observations in Altimetry were not assimilated into NCEP_Argo and NCEP_Std, they provide independent validations for the two ocean analyses. The comparison was made for SSH deviations, which were computed for Altimetry and ocean analyses separately. For Altimetry, SSH deviations were calculated with respect to the 6 year average (201.1 cm) from 2001 to 2006 over the domain 40°E –100°E and 25°S–25°N, and for NCEP_Std and NCEP_Argo, they were calculated with respect to the 6 year average of NCEP_Argo (38.5 cm) from 2001 to 2006 over the same

domain. Using the same reference for SSH deviations of both NCEP_Std and NCEP_Argo is to retain the SSH differences due to assimilation of the Argo salinity.

[31] The averaged (2001–2006) SSH deviations for Altimetry, NCEP_Std, and NCEP_Argo are shown in Figures 14a, 14b, and 14c. The mean SSH deviation of the two ocean analyses agreed very well with that of Altimetry, having an east–west SSH dipole in the equatorial Indian Ocean and a SSH minimum and maximum center in the southwestern tropical Indian Ocean. Compared to Altimetry, the mean SSH deviation of NCEP_Std is about 2–6 cm higher in the tropical Indian Ocean, the Bay of Bengal and the Arabian Sea and 2–6 cm lower in the southern Indian Ocean except near the Madagascan coasts (Figure 14d). These biases were significantly reduced by assimilating the Argo salinity (Figure 14e). The bias reduc-
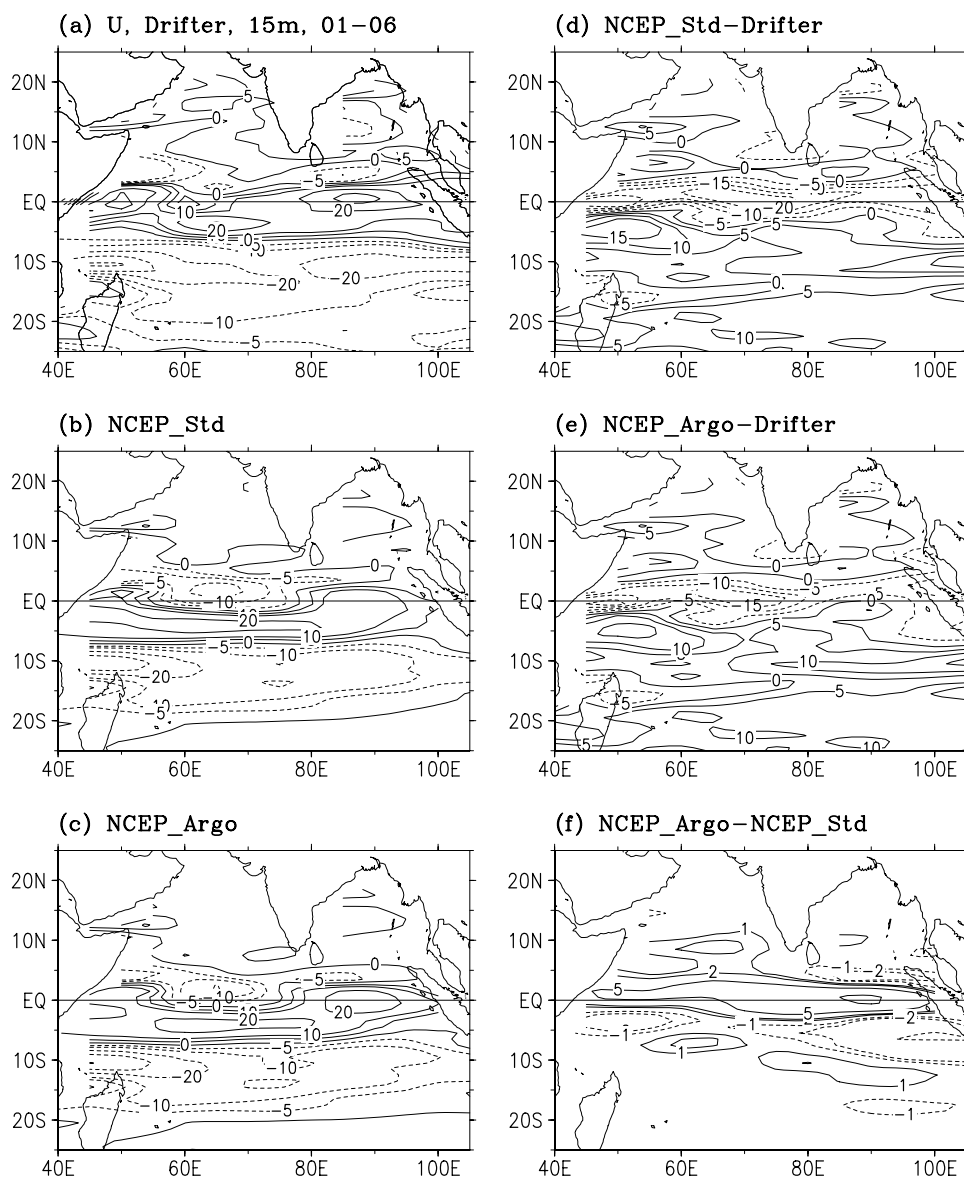
Figure 10. Averaged (2001–2006) zonal current at 15 m from (a) Drifter, (b) NCEP_Std, and (c) NCEP_Argo and zonal current difference (d) between NCEP_Std and Drifter, (e) between NCEP_Argo and Drifter, and (f) between NCEP_Argo and NCEP_Std. The contours are 0, ±5, ±10, ±20, and ±30 cm s^{-1} in Figures 10a, 10b, 10c, 10d, and 10e and ±1, ±2, ±5, and ±10 in Figure 10f.

tion was approximately 2 cm in the eastern tropical Indian Ocean, 2–3 cm in the Bay of Bengal and the Arabian Sea, and 1 cm in other regions (Figure 14f). The overall SSH reduction in the basin is due to the mean salinity increase from assimilation of the Argo salinity (Figure 3).

[32] We calculated the RMS errors between NCEP_Std and Altimetry and between NCEP_Argo and Altimetry. A negative difference between the RMS errors of NCEP_Argo and NCEP_Std (Figure 15) shows a reduction of RMS errors because of assimilation of the Argo salinity. It is seen that the RMS errors were reduced by about 1 cm in the Arabian Sea, Bay of Bengal, and tropical Indian Ocean. The reductions were most prominent in 2004 and 2005, probably because of the large areal coverage of the Argo salinity data (Figures 3 and 4). However, the reduction of RMS in 2006 was not as prominent as that in 2004 and 2005,

although the areal coverage of the Argo profiles was similar (Figure 3). In the eastern tropical Indian Ocean (Figure 16), for example, the SSH differences between NCEP_Std and Altimetry were generally larger than those between NCEP_Argo and Altimetry before July 2006 but became comparable during July December 2006 when an IOD event occurred (to be discussed further in section 5.5). As the temperature in the eastern tropical Indian Ocean decreased during the IOD event, the synthetic salinity and therefore the model salinity increased in NCEP_Std (Figure 6b), which resulted in a decrease in SSH in NCEP_Std and therefore in the bias between NCEP_Std and Altimetry. This example demonstrated that synthetic salinity may lower the model SSH to be close to observed SSH under particular circumstances, but clearly this is not always the case.
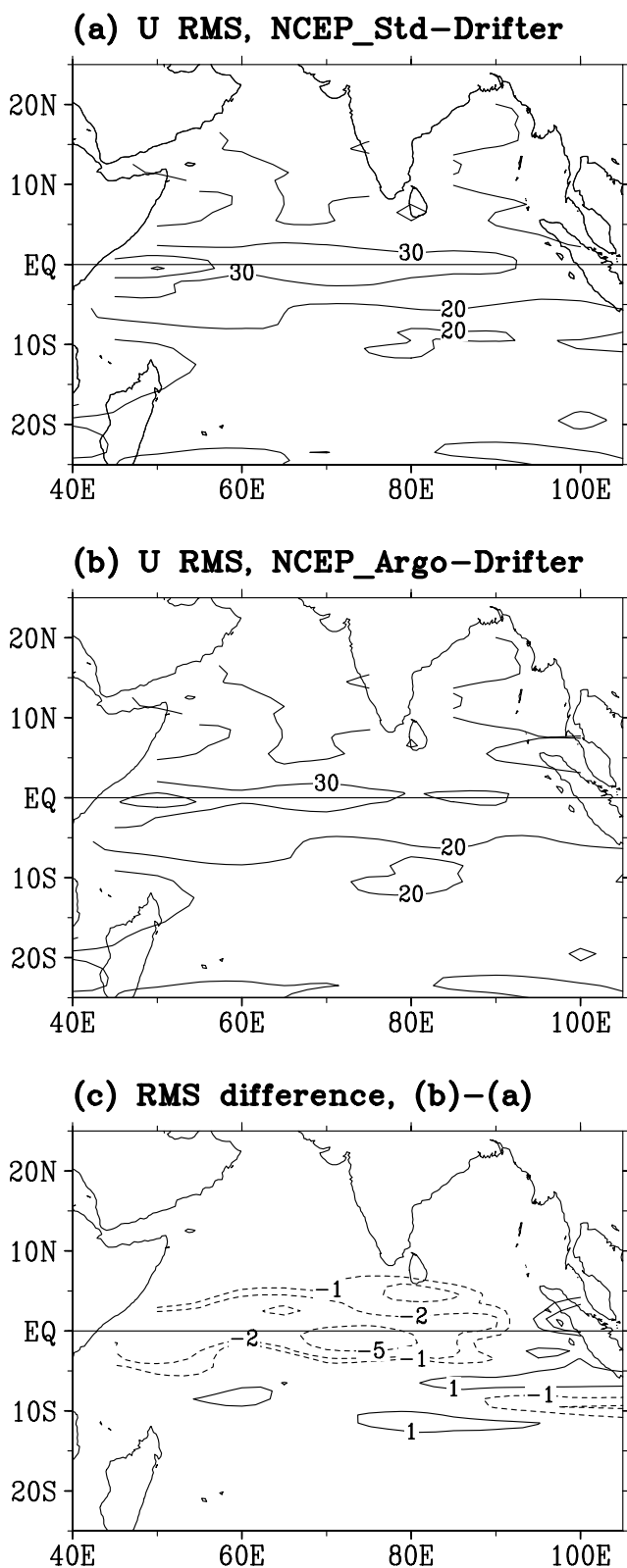
(a) U RMS, NCEP_Std−Drifter

(b) U RMS, NCEP_Argo−Drifter

(c) RMS difference, (b)−(a)

Figure 11. RMS errors of zonal current difference (a) between NCEP_Std and Drifter and (b) between NCEP_Argo and Drifter. (c) Difference in RMS errors between Figures 11b and 11a. The contour intervals are 10 cm s^{-1} in Figures 11a and 11b. The contours are ±1, ±2, and ±5 in Figure 11c.

Therefore, it is critical to replace synthetic salinity with Argo salinity whenever it is possible.

[33] To verify the seasonal-to-interannual variability of SSH, we calculated the spatial and temporal correlations between model simulations and Altimetry. The spatial correlation between NCEP_Argo and Altimetry was 1–3% higher than that between NCEP_Std and Altimetry. The temporal correlation between NCEP_Argo and Altimetry (not shown) was 5–10% higher than that between NCEP_Std and Altimetry in the eastern Arabian Sea, the Bay of Bengal, and central tropical Indian Ocean, but it was 5% lower in the northwestern Arabian Sea and central southern Indian Ocean, where the interannual variability of SSH is the largest.

5.4. An Intraseasonal Event

[34] The discussions in sections 5.1, 5.2, and 5.3 indicated that the assimilation of the Argo salinity led to a mean bias correction and RMS reduction of about 2–5 cm s^{-1} in zonal current at 15 m depth and 1–2 cm in sea surface height in the tropical Indian Ocean. However, the bias correction of zonal current can be as large as 30–40 cm s^{-1} in some periods (Figures 8 and 12). To demonstrate the potential zonal current corrections at intraseasonal timescale, the monthly average of January 2005 was chosen as an example to demonstrate the impacts of the Argo salinity on zonal current analysis.

[35] We compared model currents with OSCAR currents since there were little drifter observations in the tropical Indian Ocean in January 2005. Compared to OSCAR, NCEP_Std simulated too strong NEC near the equator in January 2005 (Figure 17a). After assimilation of the Argo salinity, the westward biases were significantly reduced (Figure 17b), and the zonal current corrections were as large as 40 cm s^{-1} (Figure 17c). The result suggests that on intraseasonal timescale, zonal current changes due to assimilation of the Argo salinity can be as large as 40 cm s^{-1}, indicating a promising role of the Argo salinity in improving the GODAS current analysis on monthly timescale.

[36] The corrections in zonal currents were associated with the corrections in SSH. The SSH of NCEP_Std was 2–5 cm too high in the tropical Indian Ocean compared to the Altimetry SSH (Figure 17d), and the biases were reduced to about 2 cm in NCEP_Argo (Figure 17e). The SSH deduction (Figure 17f) in the tropical Indian Ocean was consistent with the increase of salinity (Figure 3e) due to assimilation of the Argo salinity. Furthermore, the SSH gradient along the equator (Figure 17f) was consistent with the eastward zonal current corrections (Figure 17c). This suggests that the limited salinity observations (Figure 17f) can make significant improvements in both salinity and current analysis with an appropriate data assimilation scheme.

5.5. The 2006 IOD Event

[37] A strong IOD event and a moderate El Niño event occurred in the fall of 2006. An IOD event can have significant impacts on El Niño events according to the studies of *Shinoda et al.* [2004] and *Annamalai et al.* [2003]. Figure 18 shows the observed anomalies of SST, SSH, outgoing longwave radiation (OLR), wind stress, zonal current at 15 m, and salinity at 5 m in the tropical Indian Ocean during September–November 2006. The
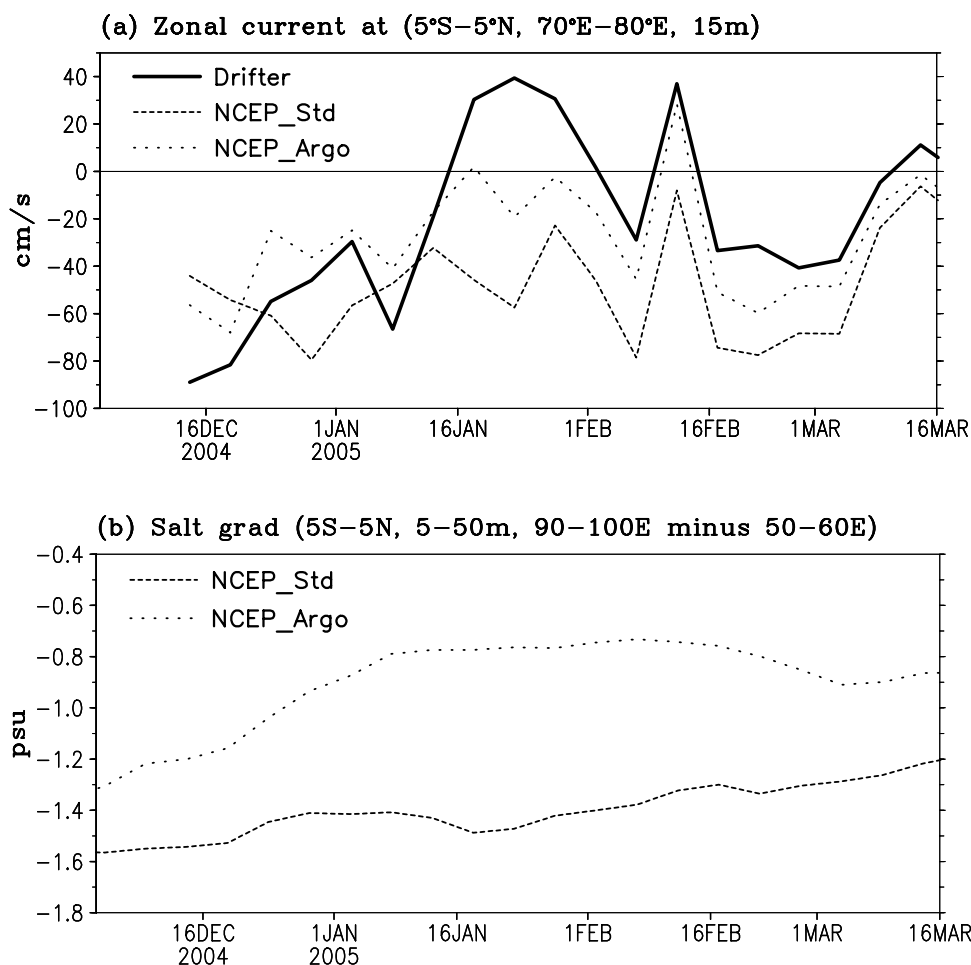
(a) Zonal current at (5°S–5°N, 70°E–80°E, 15m)

(b) Salt grad (5S–5N, 5–50m, 90–100E minus 50–60E)

Figure 12. (a) Five day-averaged zonal current (cm s^{-1}) at 15 m between 5°S and 5°N and between 70°E and 80°E in Drifter, NCEP_Std, and NCEP_Argo from December 2004 to May 2005. (b) Five day-averaged salinity gradient between the eastern (80°E–90°E, 5°S–5°N, 5–50 m) and western (50°E–60°E) tropical Indian Ocean in NCEP_Std and NCEP_Argo.
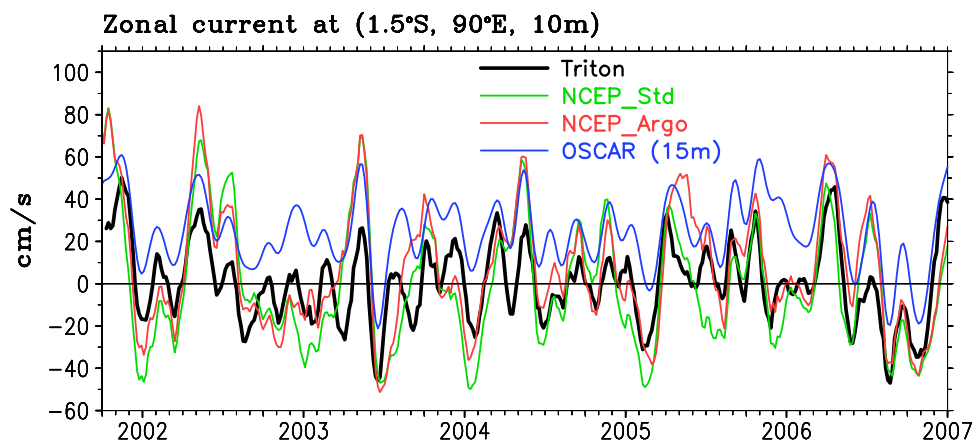
Zonal current at (1.5°S, 90°E, 10m)

Figure 13. Five day-averaged zonal current (cm s^{-1}) in TRITON, NCEP_Std, NCEP_Argo at (90°E, 1.5°S, 10 m), and Ocean Surface Current Analysis-Real Time (OSCAR) at (90°E, 1.5°S, 15 m). A 6 pentad running mean has been applied.

Table 2. Mean (2001–2006) Difference, RMS, and Correlation Coefficient in Zonal Current at (1.5°S, 90°E, 10 m) Between TRITON, NCEP_Std, NCEP_Argo, and OSCAR[a]

	Mean Difference (cm s^{-1})	RMS (cm s^{-1})	Correlation Coefficient
NCEP_Std-TRITON	−1.5	21.5	0.66
NCEP_Argo-TRITON	6.4	20.4	0.72
OSCAR-TRITON	24.2	25.9	0.86

[a]The mean zonal current is approximately 0.6 cm s^{-1} in TRITON.

sources of data are the SST data from *Reynolds et al.* [2002], the SSH data from Aviso altimetry, the OLR data from NCEP, the wind stress data from Florida State University satellite-based pseudostress [*Bourassa et al.*, 1997]

using drag coefficient from work by *Trenberth et al.* [1990], the zonal current from OSCAR, and salinity from the NCEP_Argo experiment.

[38] A strong negative SST anomaly (−2°C) was found in the southeastern tropical Indian Ocean near Sumatra and Java coasts and a weak positive SST anomaly (+0.5°C) in the west central tropical Indian Ocean (Figure 18a). Associated with the SST dipole pattern, the SSH was 5–15 cm below normal in the far eastern tropical Indian Ocean and 5–10 cm above normal in the central southern Indian Ocean (Figure 18b). Consistent with the SST anomaly, precipitation was suppressed (positive OLR anomaly) in the southeastern Indian Ocean and maritime continents and enhanced (negative OLR anomaly) in the western Indian Ocean (Figure 18c). The northwestward wind stress anomalies in
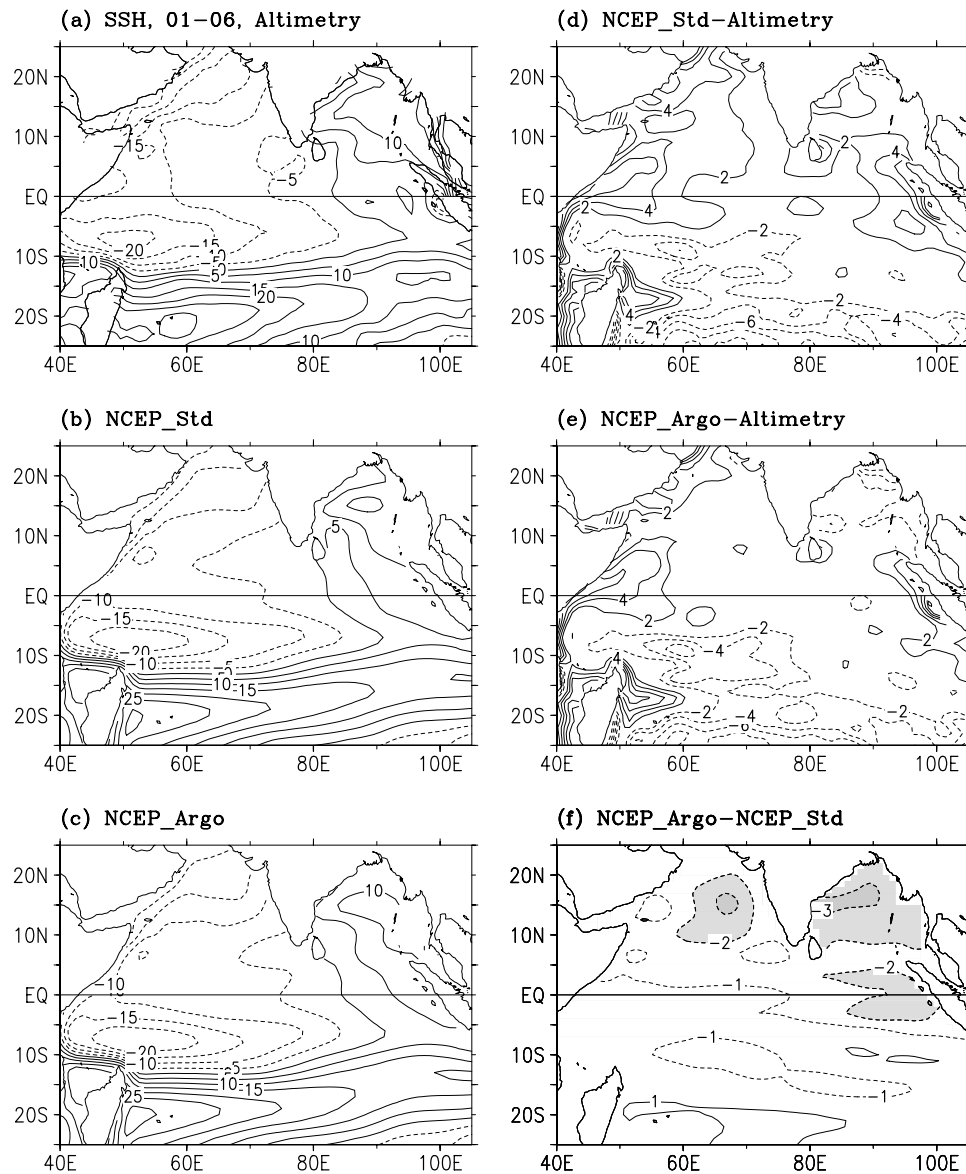

Figure 14. Averaged (2001–2006) sea surface height (SSH) in (a) Altimetry, (b) NCEP_Std, and (c) NCEP_Argo and SSH difference (d) between NCEP_Std and Altimetry, (e) between NCEP_Argo and Altimetry, and (f) between NCEP_Argo and NCEP_Std. The units are centimeters. A domain (40E°–100°E, 25°S–25°N)-averaged reference height has been subtracted in Altimetry (201.1 cm), NCEP_Std (38.5 cm), and NCEP_Argo (38.5 cm). Contours less than −1 are shaded in Figure 14f.
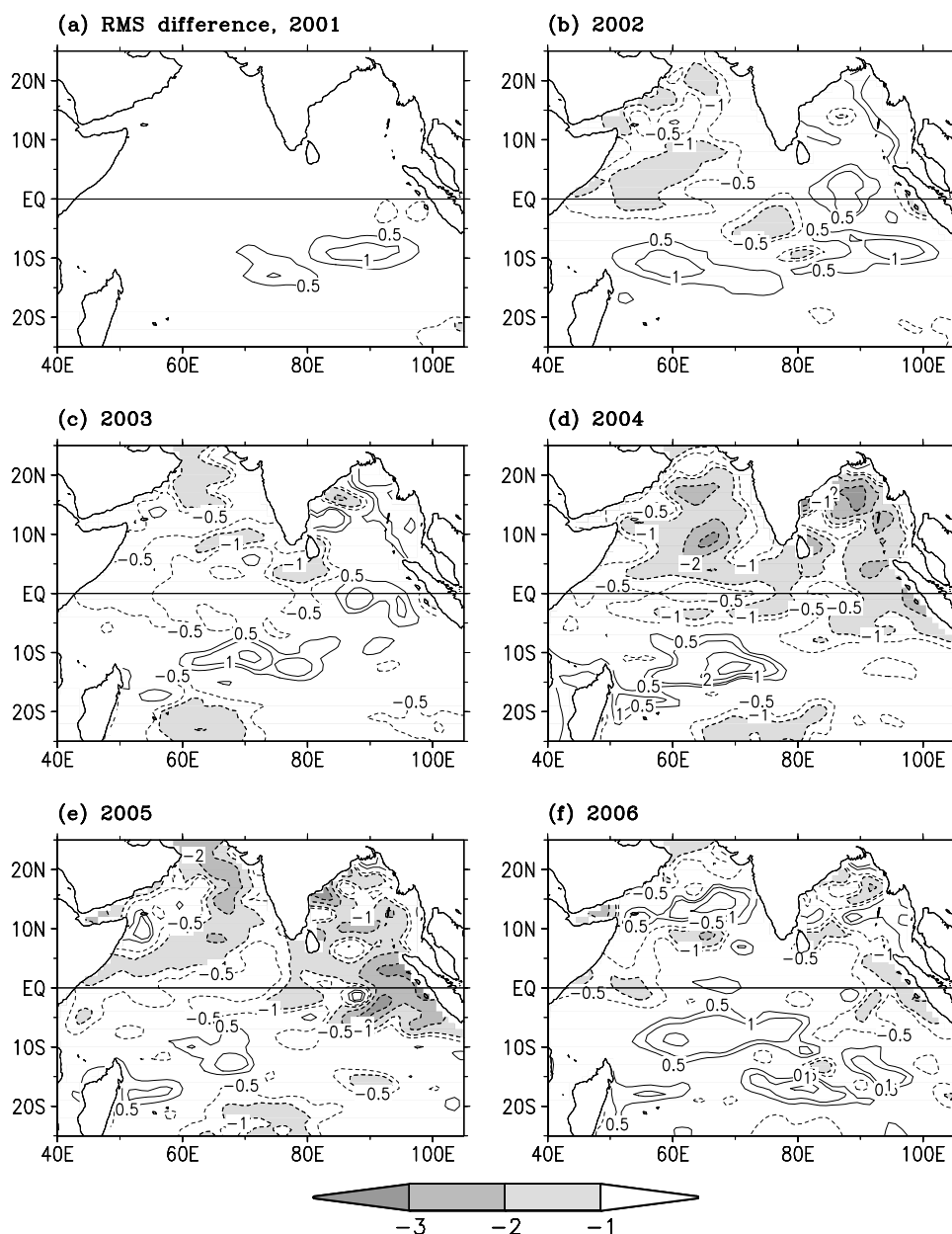
Figure 15. Difference in RMS errors of SSH in (a) 2001, (b) 2002, (c) 2003, (d) 2004, (e) 2005, and (f) 2006. The difference is defined as the RMS error between NCEP_Argo and Altimetry minus the RMS error between NCEP_Std and Altimetry. Contours are ±0.5, ±1, ±2, and ±3 cm. Contours −1, −2, and −3 are shaded.

the tropical Indian Ocean are consistent with the SST and SSH anomalies (Figure 18d).

[39] The salinity at the TRITON mooring at 90°E, 1.5°S was reduced by as much as 0.6 psu above 50 m depth during September–December 2006 (Figure 6a). Our analyses indicated that the reduction of salinity near the surface in the eastern tropical Indian Ocean (Figure 18f) was associated with an oceanic salt transport: the fresher water in the far eastern tropical Indian Ocean was advected westward by anomalous westward zonal current (Figure 18e) that was forced by the easterly wind anomalies (Figure 18d). The model salinity of NCEP_Std near the TRITON mooring had

a negative bias because of the bias in the synthetic salinity before September 2006 (Figures 2 and 6b). However, the model salinity bias switched from negative to positive after September 2006 when the TRITON salinity dropped substantially during the IOD event. In opposite to the decrease of salinity in real world, the model salinity increased during the IOD event. This was because the synthetic salinity increased when the temperature decreased in the eastern tropical Indian Ocean during the IOD event. This pointed to the drawback of assimilating synthetic salinity which does not simulate salinity variability near the surface. Once the Argo salinity was assimilated, the model salinity agreed
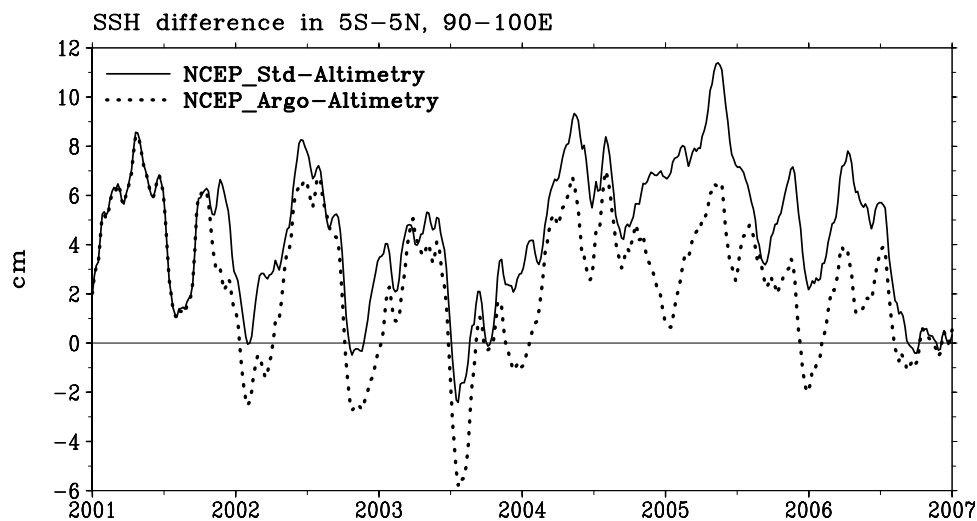
Figure 16. SSH difference (centimeters) between NCEP_Std and Altimetry and between NCEP_Argo and Altimetry in the eastern tropical Indian Ocean (5°S–5°N, 90°E –100°E).

6. Summary

[40] We analyzed the impacts of the Argo salinity on the quality of the ocean analysis produced by the NCEP's GODAS. The analysis was focused on the tropical Indian Ocean in which the quality of the GODAS ocean analysis has never been systematically validated. Our analyses were based on the two experimental GODAS runs between 2001 and 2006 that were configured similarly to the operational GODAS [*Behringer and Xue*, 2004], except they were designed to isolate the impacts of assimilation of the Argo salinity. The operational GODAS assimilates synthetic salinity that was constructed with temperature and a local climatological *T-S* correlation because salinity observations were very sparse before Argo observations became available since 2001. To isolate the impacts of the Argo salinity, one ocean analysis used the synthetic salinity, and the other replaced the synthetic salinity with the Argo salinity whenever it is available. Both ocean analyses assimilated the same temperature profiles from XBT and Argo between 2001 and 2006. The temperature profiles from TAO/TRITON/PIRATA were deliberately excluded from the two ocean analyses since their associated synthetic salinity profiles tend to overwhelm the impacts of the Argo salinity profiles, which were outnumbered by the former.

[41] The quality of the ocean analyses was verified against various independent observations such as the surface current data from drifters, the salinity and current data from the TRITON moorings, and SSH data from satellite altimeters. We found that by assimilating the Argo salinity, the biases in the salinity analysis was reduced by 0.6 psu in the eastern tropical Indian Ocean and 1 psu in the Bay of Bengal. Associated with these salinity changes, the zonal current increased $30-40$ cm s^{-1} toward the east in the central equatorial Indian Ocean during the winter seasons, while temperature changed little because of assimilating the same temperature profiles in the two ocean analyses. The

SSH biases were reduced by 3 cm in the tropical Indian Ocean, the Bay of Bengal, and the Arabian Sea. These results suggest that the Argo salinity plays a critical role in improving salinity analysis, which contributed to improved surface current and sea surface height analysis.

[42] The significant improvements in salinity, currents, and SSH between 2001 and 2006 in those two experiments demonstrated a promising role of the Argo salinity observations in improving our estimation of the state of the ocean in the NCEP GODAS. Note that our analyses covered the Argo period during $2001-2006$ when the coverage of the Argo floats varied a lot with time (Figures 1 and 4). We believe that the biases in the ocean analysis can be further reduced as more Argo observations become available in the future and more advanced data assimilation schemes are developed.

[43] Those two experiments, however, exposed the drawback of the operational NCEP GODAS that assimilates only synthetic salinity and ignores the Argo salinity observations that became available after 2001. The synthetic salinity seriously underestimated and distorted the salinity variability in intraseasonal and interannual timescales, which caused severe errors in the ocean current analysis. Our study shows that assimilation of the Argo salinity was very effective at reducing errors in the ocean currents through correcting salinity and therefore density and dynamic height. On monthly timescales, the surface currents can be modified by as much as 40 cm s^{-1} with a very limited Argo data coverage (Figure 17). This points the urgency that the synthetic salinity should be excluded from the NCEP's operational GODAS and replaced by the Argo salinity whenever they are available. However, the areal coverage of the Argo salinity may not be dense enough to ensure a good salinity analysis without help from synthetic salinity, and the synthetic salinity is definitely needed when there were little salinity observations in the period before 2001.

[44] Our analysis indicated that the bias correction in ocean currents was directly associated with a more accurate SSH analysis. We expect that the GODAS will be improved
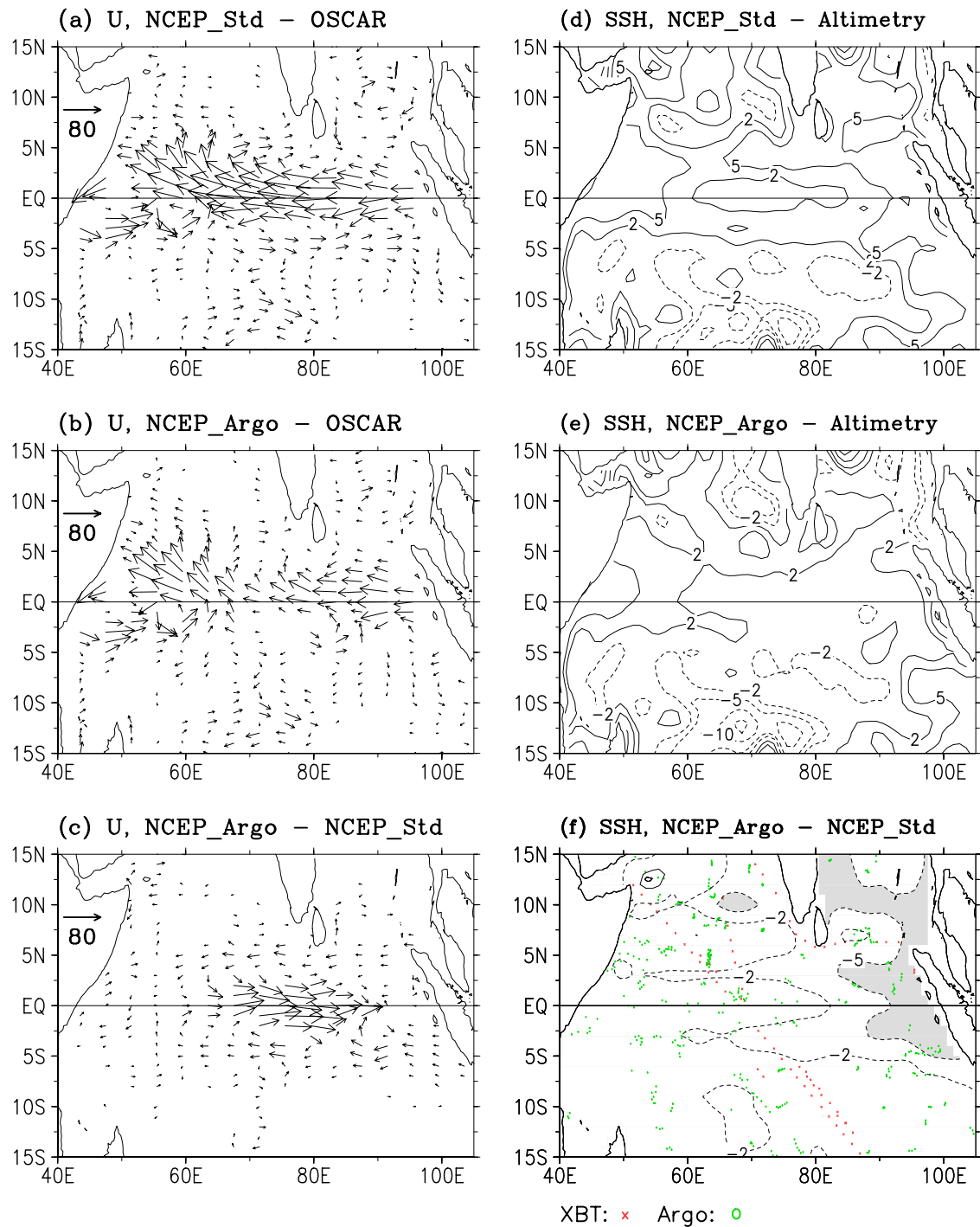
Figure 17. Differences of monthly averaged currents in January 2005 between (a) NCEP_Std and OSCAR, (b) NCEP_Argo and OSCAR, and (c) NCEP_Argo and NCEP_Std. Vector scale is 80 cm s^{-1}. Differences of monthly averaged SSH in January 2005 between (d) NCEP_Std and Altimetry, (e) NCEP_Argo and Altimetry, and (f) NCEP_Argo and NCEP_Std. Contour intervals are ±2 ± 5, ±10, and ±15 cm. The contour −5 is shaded in Figure 17f. Profiles of XBT and Argo temperature observations in January 2005 are overlapped in Figure 17f.
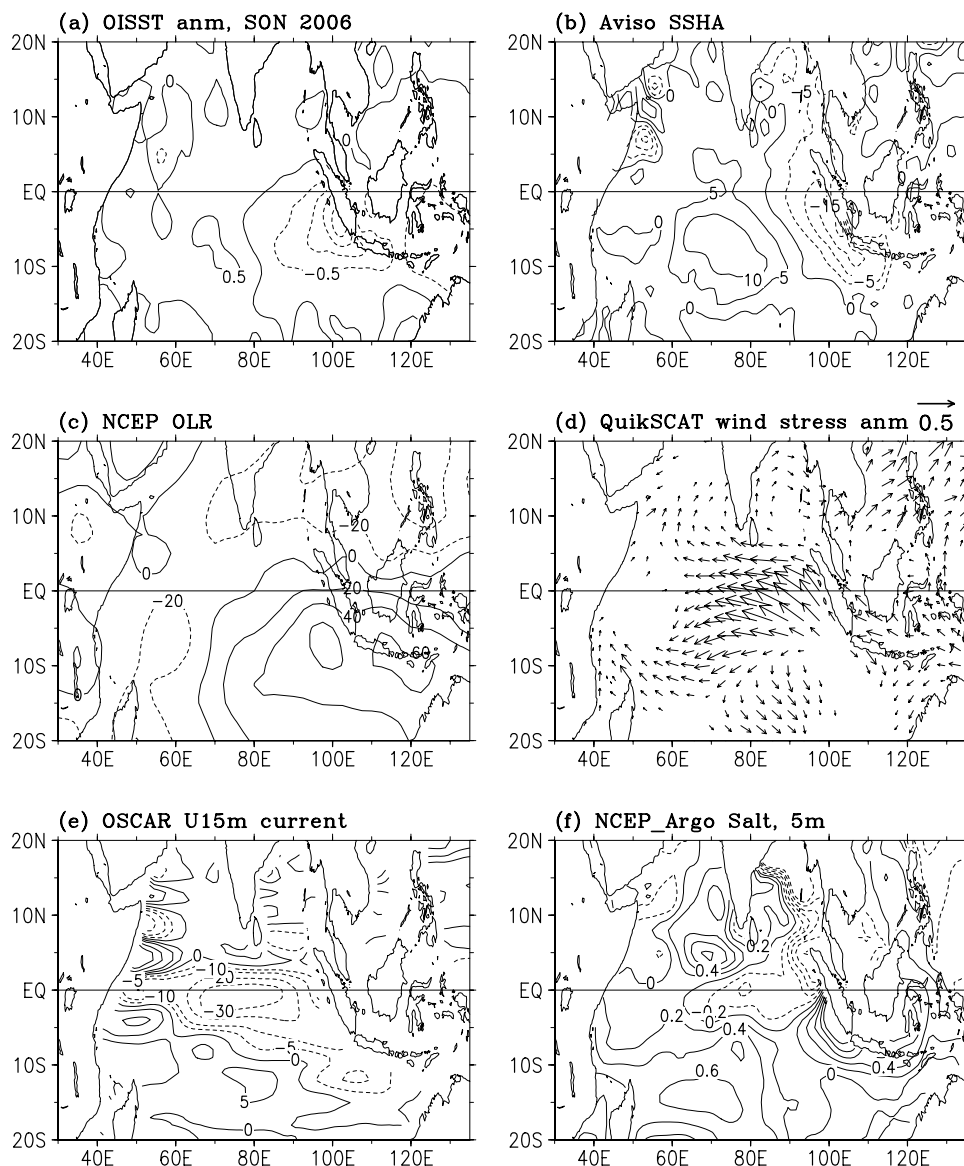
Figure 18. Averaged (September–November 2006) anomalies in (a) optimum interpolation sea surface temperature, (b) SSH, (c) outgoing longwave radiation, (d) wind stress, (e) zonal current, and (f) salinity at 5 m. Contour intervals are 0.5°C in Figure 18a, 5 cm in Figure 18b, 20 W m^{-2} in Figure 18c, and 0.2 psu in Figure 18f. Contours are 0, ±5, ±10, ±20, and ±30 cm s^{-1} in Figure 18e. Unit of wind stress is dyn cm^{-2}.

further as the Altimetry SSH and Argo salinity are both assimilated into the system. The operational GODAS was updated in April 2007 with inclusion of the Altimetry SSH but not the Argo salinity. This is because the large impact of the Argo salinity on the ocean analysis in both the Pacific [*Behringer*, 2007] and Indian oceans will potentially have a substantial impact on the seasonal forecasts of the NCEP coupled model. The change from the synthetic salinity to the Argo salinity may disrupt the calibration of the seasonal forecasts that was established by retrospective hindcasts for the 1980s and 1990s that were initialized by the operational GODAS using synthetic salinity. However, the Argo salinity will be included in the next version of GODAS, which is planed to be implemented at NCEP in 2009.

References

Acero-Schertzer, C. E., D. V. Hansen, and M. S. Swenson (1997), Evaluation and diagnosis of surface currents in the National Centers for Environmental Prediction's ocean analyses, *J. Geophys. Res.*, *102*, 21,037–21,048, doi:10.1029/97JC01584.

Annamalai, H., R. Murtugudde, J. Potemra, S. P. Xie, P. Liu, and B. Wang (2003), Coupled dynamics over the Indian Ocean: Spring initiation of

the zonal mode, *Deep Sea Res., Part II*, *50*, 2305–2330, doi:10.1016/S0967-0645(03)00058-4.

Argo Science Team (2001), The global array of profiling floats, in *Observing the Ocean in the 21st Century*, edited by C. J. Koblinsky and N. R. Smith, pp. 248–258, Aust. Bur. of Meteorol., Melbourne, Australia.

Ashok, K., Z. Guan, and T. Yamagata (2001), Impact of the Indian ocean dipole on the relationship between the Indian monsoon rainfall and ENSO, *Geophys. Res. Lett.*, *28*(23), 4499–4502, doi:10.1029/2001GL013294.

Behera, S. K., and T. Yamagata (2003), Influence of the Indian Ocean dipole on the Southern Oscillation, *J. Meteorol. Soc. Jpn.*, *81*, 169–177, doi:10.2151/jmsj.81.169.

Behringer, D. W. (2007), The Global Ocean Data Assimilation System at NCEP, paper presented at the 11th Symposium on Integrated Observing and Assimilation Systems for Atmosphere, Oceans, and Land Surface, Am. Meteorol. Soc., San Antonio, Tex.

Behringer, D. W., and Y. Xue (2004), Evaluation of the global ocean data assimilation system at NCEP: The Pacific Ocean, paper presented at the Eighth Symposium on Integrated Observing and Assimilation System for Atmosphere, Oceans, and Land Surface, Am. Meteorol. Soc., Seattle, Wash., 11–15 Jan.

Behringer, D. W., M. Ji, and A. Leetmaa (1998), An improved coupled model for ENSO prediction and implications for ocean initialization. Part I: The ocean data assimilation system, *Mon. Weather Rev.*, *126*, 1013–1021, doi:10.1175/1520-0493(1998)126<1013:AICMFE>2.0.CO;2.

Bonjean, F., and G. S. E. Lagerloef (2002), Diagnostic model and analysis of the surface currents in the tropical Pacific Ocean, *J. Phys. Oceanogr.*, *32*, 2938–2954, doi:10.1175/1520-0485(2002)032<2938:DMAAOT>2.0.CO;2.

Bourassa, M. A., M. H. Freilich, D. M. Legler, W. T. Liu, and J. J. O'Brien (1997), Wind observations from new satellite and research vessels agree, *Eos Trans. AGU*, *78*(51), 597, doi:10.1029/97EO00357.

Boutin, J., and N. Martin (2006), ARGO upper salinity measurements: Perspectives for L-band radiometers calibration and retrieved sea surface salinity validation, *IEEE Geosci. Remote Sens. Lett.*, *3*, 202–206, doi:10.1109/LGRS.2005.861930.

Conkright, M. E., et al. (1999), World Ocean Database 1998: Documentation and quality control version 2.0, http://www.nodc.noaa.gov/General/NODC-cdrom.html#wod98, Natl. Oceanogr. Data Cent., Silver Spring, Md.

Conkright, M. E., et al. (2002), World Ocean Database 2001: NESDIS 42, ftp://ftp.nodc.noaa.gov/pub/data.nodc/woa/PUBLICATIONS/wod01_1.pdf, Natl. Oceanogr. Data Cent., Silver Spring, Md.

Cooper, N. S. (1988), The effect of salinity on tropical ocean models, *J. Phys. Oceanogr.*, *18*, 697–707, doi:10.1175/1520-0485(1988)018<0697:TEOSOT>2.0.CO;2.

Derber, J., and A. Rosati (1989), A global oceanic data assimilation system, *J. Phys. Oceanogr.*, *19*, 1333–1347, doi:10.1175/1520-0485(1989)019<1333:AGODAS>2.0.CO;2.

Gent, P. R., and J. C. McWilliams (1990), Isopycnal mixing in ocean circulation model, *J. Phys. Oceanogr.*, *20*, 150–155, doi:10.1175/1520-0485(1990)020<0150:IMIOCM>2.0.CO;2.

Gould, J., et al. (2004), Argo profiling floats bring new era of in situ ocean observations, *Eos Trans. AGU*, *85*(19), 185.

Gould, W. J., and J. Turton (2006), Argo-sounding the oceans, *Weather*, *61*, 17–21, doi:10.1256/wea.56.05.

Huang, B., and V. M. Mehta (2004), The response of the Indo-Pacific warm pool to interannual variations in net atmospheric freshwater, *J. Geophys. Res.*, *109*, C06022, doi:10.1029/2003JC002114.

Huang, B., and V. M. Mehta (2005), The response of the Pacific and Atlantic Oceans to interannual variations in net atmospheric freshwater, *J. Geophys. Res.*, *110*, C08008, doi:10.1029/2004JC002830.

Huang, B., V. M. Mehta, and N. Schneider (2005), Oceanic response to idealized net atmospheric freshwater in the Pacific at the decadal timescale, *J. Phys. Oceanogr.*, *35*, 2467–2486, doi:10.1175/JPO2820.1.

Ji, M., A. Leetmaa, and J. Derber (1995), An ocean analysis system for seasonal to interannual climate studies, *Mon. Weather Rev.*, *123*, 460–481, doi:10.1175/1520-0493(1995)123<0460:AOASFS>2.0.CO;2.

Ji, M., R. W. Reynolds, and D. W. Behringer (2000), Use of TOPEX/Poseidon sea level data for ocean analyses and ENSO prediction: Some early results, *J. Clim*, *13*, 216–231.

Johnson, E. S., F. Bonjean, G. S. E. Lagerloef, and J. T. Gunn (2007), Validation and error analysis of OSCAR sea surface currents, *J. Atmos. Oceanic Technol.*, *24*, 688–701, doi:10.1175/JTECH1971.1.

Kanamitsu, M., W. Ebitsuzaki, J. Woolen, S.-K. Yang, J. J. Hnilo, M. Fiorino, and G. L. Potter (2002), NCEP-DOE AMIP-II reanalysis (R-2), *Bull. Am. Meteorol. Soc.*, *83*, 1631–1643, doi:10.1175/BAMS-83-11-1631(2002)083<1631:NAR>2.3.CO;2.

Large, W. G., J. C. McWilliams, and S. C. Doney (1994), Oceanic vertical mixing: A review and a model with nonlocal boundary layer parameterization, *Rev. Geophys.*, *32*, 363–403, doi:10.1029/94RG01872.

McPhaden, M. J., T. Delcroix, K. Hawana, Y. Kuroda, G. Meyers, J. Picaut, and M. Swenson (2001), The El Niño/Southern Oscillation (ENSO) observing system, in *Observing the Ocean in the 21st Century*, edited by C. J. Koblinsky and N. R. Smith, pp. 231–246, Aust. Bur. of Meteorol., Melbourne, Australia.

Murtugudde, R., and A. J. Busalacchi (1998), Salinity effects in a tropical ocean model, *J. Geophys. Res.*, *103*, 3283–3300, doi:10.1029/97JC02438.

Operational Oceanography Group (2006), Global Temperature-Salinity Profile Program, http://www.nodc.noaa.gov/GTSPP, Natl. Oceanogr. Data Cent., Silver Spring, Md.

Pacanowski, R. C., and S. M. Griffies (1998), MOM 3.0 manual, NOAA, Princeton, N. J.

Reynolds, R. W., N. A. Rayner, T. M. Smith, D. C. Stokes, and W. Wang (2002), An improved in situ and satellite SST analysis for climate, *J. Clim.*, *15*, 1609–1625, doi:10.1175/1520-0442(2002)015<1609:AIISAS>2.0.CO;2.

Saha, S., et al. (2006), The NCEP climate forecast system, *J. Clim.*, *19*, 3483–3517, doi:10.1175/JCLI3812.1.

Saji, N. H., and T. Yamagata (2003), Possible impacts of Indian Ocean dipole mode events on global climate, *Clim. Res.*, *25*, 151–169, doi:10.3354/cr025151.

Saji, N. H., B. N. Goswami, P. N. Vinayachandran, and T. Yamagata (1999), A dipole mode in the tropical Indian Ocean, *Nature*, *401*, 360–363.

Schott, F. A., and J. P. McCreary (2001), The monsoon circulation of the Indian Ocean, *Prog. Oceanogr.*, *51*, 1–123, doi:10.1016/S0079-6611(01)00083-0.

Shinoda, T., H. H. Hendon, and M. A. Alexander (2004), Surface and subsurface dipole variability in the Indian Ocean and its relation with ENSO, *Deep Sea Res., Part I*, *51*, 619–635, doi:10.1016/j.dsr.2004.01.005.

Sprintall, J., and M. Tomczak (1992), Evidence of the barrier layer in the surface layer of the tropics, *J. Geophys. Res.*, *97*, 7305–7316, doi:10.1029/92JC00407.

Trenberth, K. E., W. G. Large, and J. G. Olson (1990), The mean annual cycle in global ocean wind stress, *J. Phys. Oceanogr.*, *20*, 1742–1760, doi:10.1175/1520-0485(1990)020<1742:TMACIG>2.0.CO;2.

Vialard, J., P. Delecluse, and C. Menkes (2002), A modeling study of salinity variability and its effects in the tropical Pacific Ocean during the 1993–1999 period, *J. Geophys. Res.*, *107*(C12), 8005, doi:10.1029/2000JC000758.

Woodgate, R. A. (1997), Can we assimilate temperature data along into a full equation of state model?, *Ocean Modell.*, *114*, 4–5.

Wyrtki, K. (1973), An equatorial jet in the Indian Ocean, *Science*, *181*, 262–264, doi:10.1126/science.181.4096.262.

————————————

D. W. Behringer, EMC, NCEP, NOAA, Room 807, 5200 Auth Road, Camp Springs, MD 20746, USA.

B. Huang and Y. Xue, CPC, NCEP, NOAA, WWB Room 605-A, 5200 Auth Road, Camp Springs, MD 20746, USA. (boyin.huang@noaa.gov)